EXPERIMENTAL INVESTIGATION OF SIZE EFFECT ON THERMAL CONDUCTIVITY FOR ULTRA-THIN AMORPHOUS POLY(METHYL METHACRYLATE) (PMMA) FILMS

A Thesis

by

ICK CHAN KIM

Submitted to the Office of Graduate Studies of
Texas A&M University
in partial fulfillment of the requirements the degree of

MASTER OF SCIENCE

May 2007

Major Subject: Mechanical Engineering

EXPERIMENTAL INVESTIGATION OF SIZE EFFECT ON THERMAL CONDUCTIVITY FOR ULTRA-THIN AMORPHOUS POLY(METHYL METHACRYLATE) (PMMA) FILMS

A Thesis

by

ICK CHAN KIM

Submitted to the Office of Graduate Studies of
Texas A&M University
in partial fulfillment of the requirements the degree of

MASTER OF SCIENCE

Approved by:

Chair of Committee,	Egidio E. Marotta
Committee Member,	N.K. Anand
	Tahir Cagin
Head of Department,	Dennis L. O'Neal

May 2007

Major Subject: Mechanical Engineering

ABSTRACT

Experimental Investigation of Size Effect on Thermal Conductivity for Ultra-thin Amorphous Poly(methyl methacrylate) (PMMA) Films. (May 2007)

Ick Chan Kim, B.En., In-Ha University

Chair of Advisory Committee: Dr. Egidio E. Marotta

An investigation was conducted to determine whether a "size effect" phenomenon for one particular thermophysical property, thermal conductivity, actually exists for amorphous poly(methyl methacrylate) (PMMA) films with thicknesses ranging from 40 nm to 2 μm. This was done by using a non-contact, non-invasive, in-situ Transient Thermo-Reflectance (TTR) laser based technique. The results demonstrated that the intrinsic thermal conductivity of a 40 nm PMMA film deposited on native oxide of silicon increases by a factor of three over bulk PMMA values, and a distinct increase in the thermal conductivity of PMMA film was observed in ultra-thin (sub 100 nm) films. This confirmed the importance of film thickness for the through-plane thermal conductivity value of PMMA film on native oxide of silicon.

DEDICATION

To Keumsil Kang and Courtney Kim

ACKNOWLEDGEMENTS

I would like to thank my committee chair, Dr. E. E. Marotta, and my committee members, Dr. N. K. Anand and Dr. Tahir Cagin, for their guidance and support throughout the course of this research.

Special appreciation must go to Dr. Mihai G. Burzo, Dr. Pavel L. Komarov, and Dr. Peter E. Raad for their help in experimental accomplishment, valuable suggestions, and significant advice. I also deeply appreciate their kindness that allowed me to use the apparatus of the Nanoscale Electro-Thermal Laboratory (NETSL).

Many thanks go out to Dr. Yulia Vasilyeva, Dr. Orla Wilson, and Dr. William Lackowski for their advice and helping me use the experimental apparatus in the Materials Characterization Facility (MCF) Laboratory. I deeply appreciate the very kind and helpful advice of Dr. Jaime Grunlan for the scientific study of polymeric film.

I would particularly like to thank Dr. Michael Pendleton and Mr. Tom Stephens for their advice and help in using the apparatus of the Microscopy and Imaging Center (MIC).

Thanks also to my friends and colleagues and the department faculty and staff for making my time at Texas A&M University a great experience.

Finally, thanks to my wife and daughter for their encouragement, patient support, and love.

TABLE OF CONTENTS

CHAPTER Page

LIST OF FIGURES

FIGURE Page

LIST OF TABLES

NOMENCLATURE

A_j	=	atomic mass
$A_{PMMA,\,K}$	=	thermal conductivity measurement area in a sample
$A_{gold,\,h}$	=	thickness measurement area of the deposited gold layer
$A_{PMMA,\,h}$	=	thickness measurement area of PMMA film
c_j	=	number fraction
C_p	=	specific heat at constant pressure [J kg^{-1} K^{-1}]
C_v	=	specific heat at constant volume per unit volume [J m^{-3} K^{-1}]
Con	=	concentration of solution [%]
D_{max}	=	dimension of the heating spot [m]
E	=	Young's modulus [GPa]
F	=	fluence of the heating laser [J m^{-2}]
Fo	=	Fourier non-dimensional number
H	=	dimensionless film thickness
h	=	film thickness [m]
I	=	heating irradiation intensity [W m^{-2}]
K	=	thermal conductivity [W m^{-1} K^{-1}]
K_{PMMA}	=	intrinsic (internal) thermal conductivity of the PMMA film [W $m^{-1}K^{-1}$]
k	=	extinction coefficient (imaginary part of the refractive index)
l	=	carrier mean free path [m]
n	=	real part of the refractive index

N_a = Avogadro's number

$\dot{Q}$ = heat source [W m^{-3}]

R = surface reflectivity

R_I = interface thermal resistance [m^2 K W^{-1}]

R_{th} = total interface thermal resistance [m^2 K W^{-1}]

T = temperature [K]

$T_{ambient}$ = ambient temperature [K]

T_{chuck} = thermochuck isothermal temperature [K]

T_g = glass transition temperature [K]

t = time [s]

t_0 = maximum light intensity time [s]

V = volume [m^3]

v = average carrier velocity [m s^{-1}]

w = absolute uncertainty

W = relative uncertainty [%]

Z = dimensionless coordinate

Z_j = atomic number

Greek Symbols

α = thermal diffusivity [m^2 s^{-1}]

ΔL = light penetration depth [m]

ΔT = temperature gradient [K]

Δt	=	time gradient [s]
δ_H	=	heat penetration depth during the heating pulse [m]
λ	=	radiation wavelength [m]
θ	=	dimensionless temperature
ρ	=	mass density [g cm^{-3}]
ρ_e	=	electronic density [e $Å^{-3}$]
σ	=	standard deviation
γ	=	absorption coefficient
τ	=	pulse width of the heating laser [s]
Ω	=	responsivity

Subscripts

ab	=	absorption
bulk	=	Bulk material
e	=	average electron property at Fermi levels
exp	=	experimental
h	=	thickness
num	=	numerical
r,z	=	Direction indices
s	=	average phonon property

CHAPTER I

INTRODUCTION

1.1 Objectives

There are numerous applications for the use of ultra-thin polymeric films such as nano-scale lithography, thermo-mechanical data storage media, and lubricating coatings. As technology proceeds towards smaller and higher density microelectronic devices, one will face an atomic-scale dimensions that deviate from continuum. Since mechanical and chemical properties of ultra-thin polymeric films can vary dramatically from their bulk value, depending on the dimension of the film and on the properties of the film's substrate, thermophysical properties for thin films are also expected to vary.

Ultra-thin poly(methyl methacrylate) (PMMA) films have been the focus of numerous investigations in recent years as a data storage media. Employing Atomic Force Microscopy (AFM) technology, research scientists[1-3] have stored data bits by heating, and then melting a target zone, which leaves a nano-dimple indentation in the PMMA polymer film. AFM based data storage technology has great potential because it possesses considerable data density when compared to conventional magnetic data storage. However, knowing the precise thermophysical properties in ultra-thin PMMA films is a critical factor in advancing this new storage technology.

This thesis follows the style of International Journal of Heat and Mass Transfer.

A goal for this investigation was to determine whether any dependence exists between film thickness and thermal conductivity for PMMA thin films deposited on a silicon substrate that contains a native oxide. Commonly, heat carriers such as electrons and phonons in metallic and dielectric materials, respectively, are influenced by the "size effect" in micro-scale dimensions. Experimental investigations for the size effect on thermophysical properties in dielectric or metallic materials have been reported from a large number of researchers. Although thin polymeric films have played an important role in many microelectronic devices; property data at nano-length scales for polymeric materials are still insufficient to satisfy microelectronic applications.

Therefore, this study evaluated the "size effect" on an important thermophysical parameter, the intrinsic through-plane thermal conductivity, for PMMA films with thicknesses that ranged from 40 nm to 2 μm. The Transient Thermo-Reflectance (TTR) system by Burzo et al.[4] was used to quantitatively measure the through-plane thermal conductivity of PMMA films as the thickness of the film was varied.

1.2 Outline

Chapter II, which follows, shows a brief literature review of the experimental work on thermal conductivity for very thin films and the mechanical and chemical characteristics of the PMMA films. Chapter III gives an account of the experimental set up for this research, including sample preparation for the various thicknesses of the PMMA films. The results and uncertainty of this experiment are described in Chapter

IV. The summary and conclusions from this research and future works are presented in Chapter V.

CHAPTER II

LITERATURE REVIEW

2.1 Microelectronic Application

IBM Research (Zurich Research Laboratory), Durig et al.[3] and King et al.[5] have studied the new technology of data storage that was mentioned in the previous chapter. Employing Atomic Force Microscopy (AFM) technology with ultra-thin Poly(methyl methacrylate) (PMMA) film as data storage media, they presented considerably increased data density when compared to conventional magnetic data storage. Magnetic data storage technology faces a limitation when data density nears 100 $Gbit/in^2$, owing to a super-paramagnetic effect which governs the thermal stability of a magnetic data bit[3,5,6].

However, AFM based data storage technology has demonstrated data densities of up to 500 $Gbit/in^2$[3], and has achieved a data rate of 6 *Mbit/s* with a single AFM tip[7]. Moreover, employing a MEMS device with 1024 cantilevers in a 32 × 32 square array, King et al. predicted that data storage rates up to 500 *Mbit/s* were practicable, and even rates beyond 10 *Gbit/s* could be expected. PMMA films play an important role as the data media for thermomechanical writing, reading, and erasing of the nano-indentations with dimple pitches of 30-40 *nm*[1,2]. Nevertheless, to ascertain greater data densities and pitch dimensions, precise thermal conductivity values for the PMMA film are required as a function of film thickness.

King and Goodson[8] described the data writing and erasing with a heated AFM cantilever tip on polymer media illustrated as Fig. 2.1. Contacting with and scanning over a thin polymer film, the heated cantilever tip induces the thermomechanical formation of nanometer-sized indentations in the polymer. In addition, erasing or modifying the indentations is accomplished by applying the heated tip just beside the previous written indentations. The volume of the melted polymer bit that was depicted as a red colored area in Fig. 2.1 might be considered as a remaining research field since the size of the melted volume should be controlled in order to protect other indentations that must be kept as data. This fact was also found in the tracks of thermally written indentations with different periodicity. As King and Goodson[8] reported, the thermal diffusion and melted polymer flow influences neighboring indentations as the indentation periodicity increases in the polymer layer as illustrated in Fig. 2.2. One can see that indentations highly influence each other in the area of maximum data density (right side column), which is 0.9 Tbit/in^2.

One of the parameters that affect the size of the volume is the thermal conductivity of the polymer media; however, the thermal property varies depending on the thickness of the polymer film that is nanometer-scaled thickness. This thermophysical property is a critical issue in increasing the data density and rate in AFM data storage technology. Precise knowledge of the effect on thermal properties can lead to a more precise prediction of the melting zone[8], in this case the film volume which creates a data bit, and thus provide a more accurate dwelling time for the heating and melting of the nano-indentations.

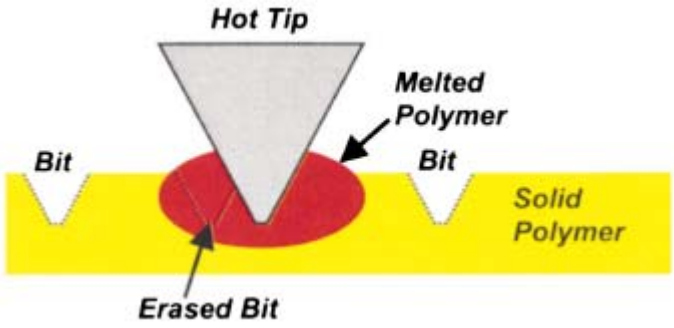

Fig. 2.1 Schematic of thermal writing and erasing data bits on solid polymer media by King and Goodson [8]

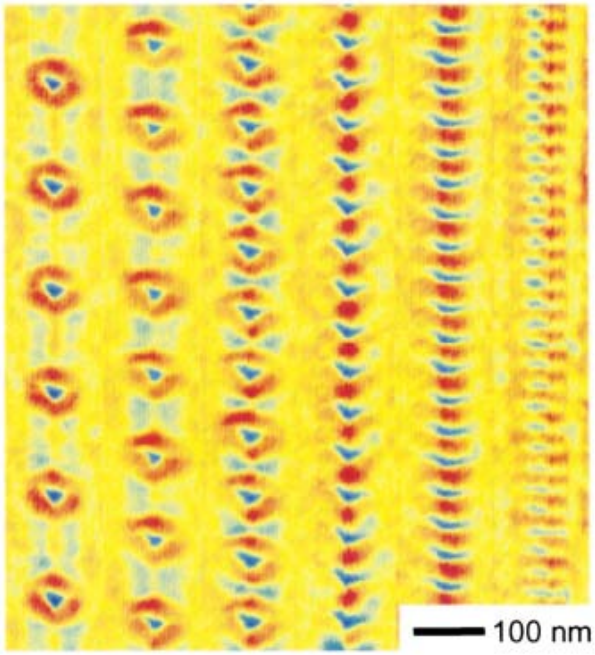

Fig. 2.2 Tracks of thermally written indentations in a thin polymer layer: from lower data density (left column) to maximum data density (right column) by King and Goodson [8]

2.2 Material Property Measurements for PMMA Film

Based on kinetic theory, the thermal conductivity for a solid can be calculated as follows, Rohsenow and Choi[9], Cahill et al.[10], and Omar, M. A.[11]:

$$K = \frac{1}{3} C_v v l \tag{2.1}$$

where K is the thermal conductivity, $C_v = C_s$ is the phonon specific heat per unit volume, $v = v_s$ is the averaged acoustic speed, and $l = l_s$ is the phonon mean free path in for dielectric materials. For thermal conduction in metals, $C_v = C_e$ is the electronic specific heat per unit volume, $v = v_e$ is the electron speed at Fermi levels, and $l = l_e$ is the electron mean free path at Fermi levels. Having investigated thermal properties of metallic and dielectric materials based on Eq. (2.1), researchers have shown a "Size Effect" in ultra-thin (sub 100 nm) and thin (sub 1 μm) films. Flik et al.[12] showed that boundary scattering increases with ratio l/h, where l is the bulk value of the mean free path of the heat carriers and h is the film thickness in metallic and dielectric materials.

If the film thickness h is less than or approaches l, the effect of boundary scattering must be considered while the volume resistance of the film may be neglected when $l << h$. Moreover, they showed that the microscale regime criteria has to be used for thermal conduction in both metallic and dielectric films if $h < 7l$, which is the dimension that separates the microscale and macroscale regimes. However, very little data exist in the literature for thermal conductivity of thin organic films, and the regime map that is attributed to dimensions up to ultra-thin thicknesses has not been investigated.

2.2.1 Mass Density of PMMA Film with Various Film Thicknesses

In order to calculate the mean free path of the acoustic phonon in a polymer film, other properties of the material had to be determined. Van der Lee et al.[13] presented mass density profiles for intrinsic PMMA films that relied on their experimental investigation of the electron density profiles normal to the substrate. Film thicknesses between 20-80 nm for stereoregular PMMA were spin-cast on (111) silicon surfaces, and then X-ray analyzed with reflectomertry. They calculated the mass density, $\rho(z)$, from the electronic density, $\rho_e(z)$, as follows:

$$\rho(z) = \frac{\rho_e(z)\sum_j c_j A_j}{N_a \sum_j c_j Z_j} \tag{2.2}$$

where A_j, Z_j, and c_j are the atomic mass, the atomic number, and the number fraction, respectively, of element j in the chemical formula of the polymer, and N_a is the Avogadro's number.

Depending on the thickness of the film the average mass density, reported in Table 2.1, was obtained by taking the density of 1.9 g/cm^3 as representative of the film/silicon interface since the density of the native oxide layer on silicon was 1.9 g/cm^3. Their results showed that the calculated densities in the thickness range were higher than the bulk density of amorphous PMMA, which is 1.19 g/cm^3.

Table 2.1 Mass density of ultra-thin PMMA film with two different tacticity versus film thickness by van der Lee et al.[13]

Thickness of film	Film/Silicon Interface	20 nm	35 nm	70 nm	Bulk PMMA
Average Density (g/cm^3) of isotactic PMMA	1.9	1.32	1.28	1.25	1.19
Average Density (g/cm^3) of syndiotactic PMMA		1.28	1.25	1.24	

The authors concluded that the PMMA's density increases when the film thickness decreases and the density of isotactic PMMA is always higher than that of syndiotactic PMMA. They suggested that the reasons, why the mass density increases with decreasing thickness, were possibly due to the attractive interaction that was attributed to hydrogen bonding between the PMMA film and the native oxide on the silicon substrate. The correlation between these results with the glass transition temperature, T_g, depending on various substrates, was found in the study by Keddie et al. [14]

2.2.2 Glass Transition Temperature (T_g) in PMMA Film on Two Different Substrates

Using spectroscopic ellipsometry to detect the discontinuity in thermal expansivity occurring at the glass transition temperature (T_g), Keddie et al.[14] measured the thickness dependence of T_g in thin films of PMMA. They compared the dependence by varying PMMA film thickness on two different substrates: on native oxide of silicon surface (111) and on an evaporated gold layer. They varied the film thickness by changing the concentration of the solution and determined the T_g by finding the discontinuity in thermal expansivity when the thin film sample was heated from room temperature at a rate of 2 K min^{-1}.

Considering thickness dependence and the effects of polymer-substrate interaction on the mobility of thin polymer films, they concluded that the T_g of the PMMA on the gold surface decreases with decreasing film thickness while the T_g of the PMMA on the surface of the native oxide of silicon increases with decreasing film thickness. They suspected that the reason for the effects could be the restriction of the mobility of polymer chains along the interface where hydrogen bonding exists between the PMMA and surface hydrogen groups. The results of the measurement of T_g in the PMMA films on the Au layer and on the native oxide of silicon wafer are illustrated in Fig. 2.3 and Fig. 2.4.

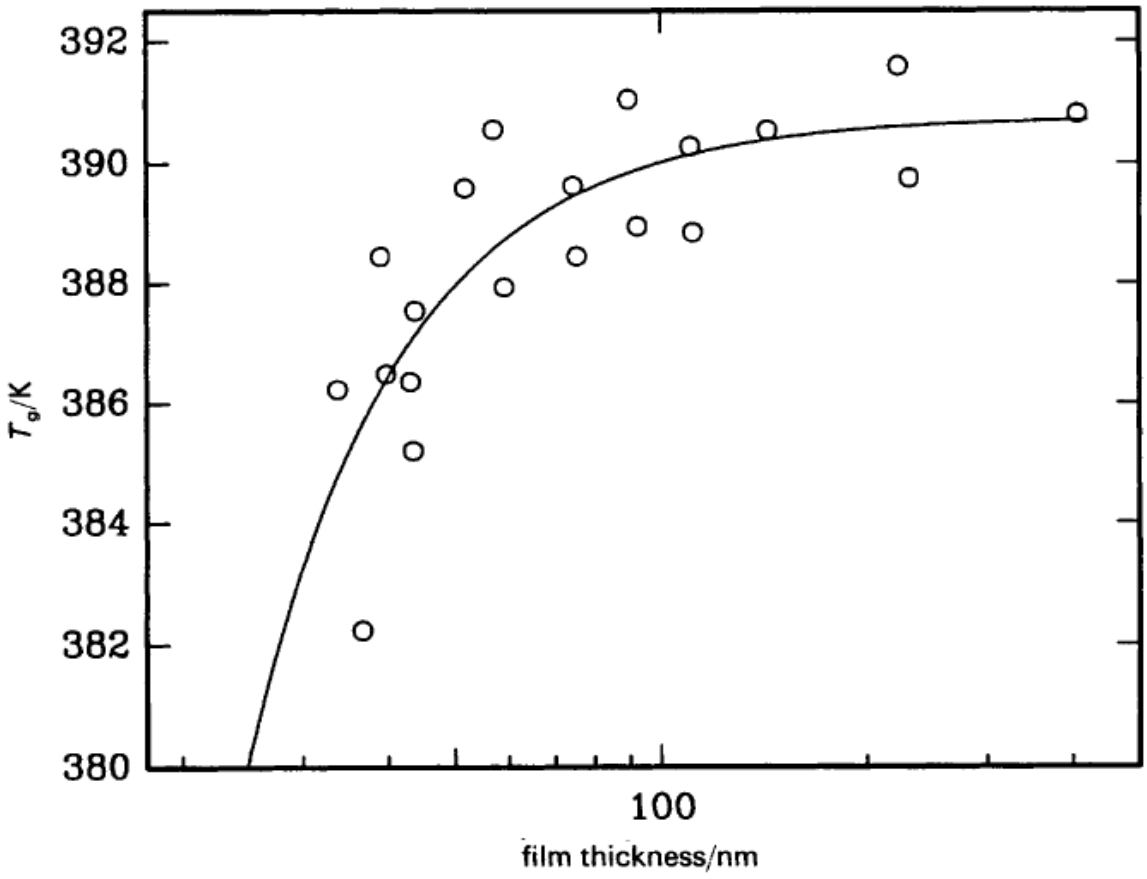

Fig. 2.3 T_g for PMMA films on the Au layer depending on PMMA film thickness by Keddie et al.[14]

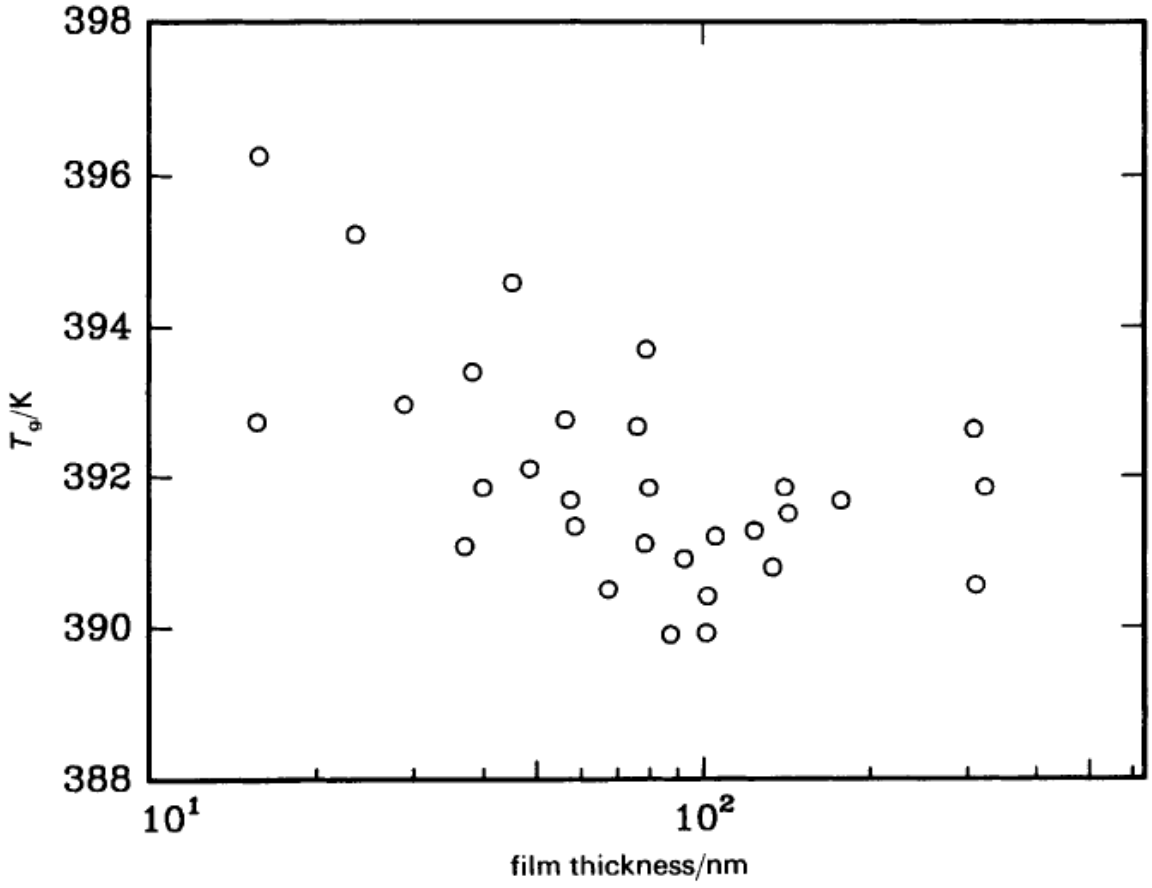

Fig. 2.4 T_g for PMMA films of the native oxide of silicon wafer depending on PMMA film thickness by Keddie et al. [14]

Fryer et al.[15] also studied the dependence of thickness and interfacial energy between PMMA films and substrate for glass transition temperature. They showed that the deviation of the T_g values for the thin films when compared to the bulk values increased with decreasing film thickness at high interfacial energy between polymer film and substrate. The T_g of the polymer films was less than the corresponding bulk value at low values of the interfacial energy. Diakoumakos, C. D. and Raptis, I.[16] measured the T_g of PMMA films that were spin-coated onto untreated silicon substrates, and they did not observe considerable differences in T_g values of PMMA films with thickness higher than 200-250 nm. However, they observed that the T_g of PMMA films increased by decreasing film thickness under 200 nm. Moreover, they reported that the T_g of ultrathin (sub-100 nm) PMMA film was significantly increased and deviated substantially by approximately 30 ˚C from the bulk value of PMMA film.

They also suspected that hydrogen bonding between the polymer film and the native oxide of the substrate. Generally, polymer materials that have high values for the Young's modulus show trends of high glass transition temperatures (T_g). Thus, one may suspect the T_g in thin PMMA films are related with the average sound speed in the film. In addition, the restriction of the polymer chain's mobility may be related to the local molecular packing, which affects mass density of the polymer near the interface between the polymer and substrate.

2.2.3 Through-plane Acoustic Speed of PMMA Film

Lee et al.[17] experimentally measured the longitudinal wave speed for PMMA films of thicknesses ranging from 20 to 130 nm by applying a picosecond acoustic technique in the through-plane direction. Since this acoustic speed is directly related to the thermal conductivity in Eq. (2.1) as well as to the Young's modulus and the mass density of the thin film, its measurement for thickness dependence and substrate effect must be considered when analyzing thermal conductivity.

They chose a highly absorbing aluminum film transducer in order to absorb the laser pulse energy and to generate an acoustic pulse. The bare aluminum transducer film with a thickness of 13 nm was deposited on (100) silicon substrates, and then PMMA films were spin-cast onto the Al/Si substrate by varying the PMMA solution concentration. Measuring the roundtrip time-of-flight of the acoustic wave and the film thickness, they calculated the longitudinal wave velocities for PMMA films and plotted the data as shown in Fig. 2.5.

The measured acoustic speed increased to 7000-8000 m s^{-1} for PMMA films between 20-25 nm thick and 3000 m s^{-1} at 40 nm thick, while the measured wave speed agreed well with bulk speed of 2700 m s^{-1} in PMMA films of thicknesses greater than 40 nm. They also compared the acoustic speeds in PMMA films deposited on oxide layers, Al_2O_3, and found a 10%-20% increase in the longitudinal wave speed for films thinner than 60 nm.

Although the author mentioned that the wave speed variation could be attributed to the uncertainty of the thickness measurement by ellipsometry, the substrate effect due

to Al_2O_3 can not be overlooked since the mass density and glass transition temperature of the PMMA films showed the substrate effect as well as thickness dependence.

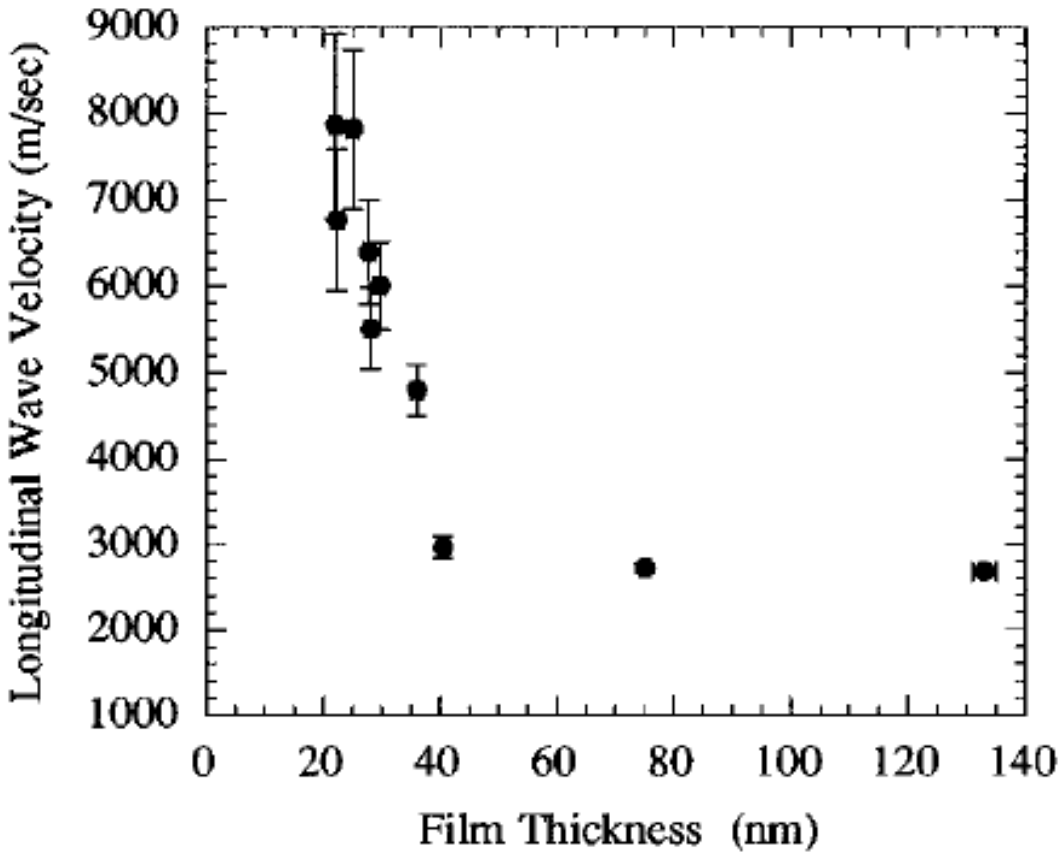

Fig. 2.5 The measured longitudinal wave velocity versus film thickness in PMMA films on aluminum layer by Lee et al. [17]

2.2.4 Elastic Modulus of PMMA Film

As mentioned, it appears that the interfacial interaction between polymer films and substrates undoubtedly affects the mechanical properties of the thin films, especially in ultra thin films such as those below 40 nm. There have been numerous trials to measure the mechanical properties and structures of thin films by a number of experimental methods such as nano-indentation; however, measurement methodology for direct contact still remains challenging for ultra thin films.

For example, soft materials such as polymer films present difficulty in applying the indentation due to creep concerns and the uncertainty of contact area at the tip of the nano-indenter. Introducing a new measurement method called "buckling-based metrology" that can be applied to nanoscale polymer films for elastic moduli, Stafford et al.[18,19] investigated the elastic moduli of ultra-thin poly(styrene) (PS) and poly(methyl methacrylate) (PMMA) films of thicknesses ranging from 200 nm to 5 nm. According to their results, the apparent modulus as a function of thickness in the PS and PMMA films decreased by an order of magnitude when compared to bulk values for the thinnest films measured.

Although the apparent modulus was expected to increase according to the measured T_g and acoustic wave speed for ultra thin PMMA films, deposited on native oxide of the silicon substrate, their results showed an opposite trend. This was attributed to the fact that the substrate used for the modulus measurement did not have a native oxide layer. In the sample preparation for the buckling-based metrology, Stafford et al.[19] first spin-casted polymer films onto silicon wafers, and then the films were

transferred from the silicon wafers onto relatively soft elastic substrates of prestrained polydimethylsiloxane (PDMS) via a water immersion technique. Therefore, it remains difficult to apply their modulus data to the result for the acoustic wave speed determined by Lee et al.[17]. This is due to the fact that the transferred films are expected to have substrate effects not attributable to the aluminum layer on silicon wafer or the native oxide on aluminum layer, but to a relatively soft elastic PDMS layer.

2.2.5 Thermal Properties in PMMA Film

Frank et al.[20] reported that the thermal conductivity of PMMA films with 40 μm, 26 μm, and 5 μm thicknesses were found to be 0.1888 ± 0.006 W m^{-1} K^{-1} , which was independent of the film thickness. Using the 3ω/decay technique based on a "plane-source technique," they measured the thermal conductivity of the PMMA films on an aluminum substrate with specific heat C_p = 1440 J kg^{-1} K^{-1} and mass density ρ = 1180 kg m^{-3}. Their results were basically in agreement with the value of bulk PMMA because it is usually hard to anticipate thickness or substrate effects in films with thicknesses over 1 μm. For thinner films, Chu et al.[21] tried to measure the thermal conductivity of PMMA films with 400 nm thickness by applying the thermo-reflectance method, which is very similar to the TTR method used in this study. The reported thermal conductivity was 0.16 ± 0.03 W m^{-1} K^{-1}, which was slightly less than bulk value.

However, one may question the sample preparation for the thermo-reflectance method since an aluminum layer was used for the top layer of the samples and aluminum is very easily oxidized. Burzo et al.[22] reported the importance of the top layer in

absorbing the heating laser irradiation and for reflectivity due to surface temperature change since the weak responsivity of the surface temperature provides considerable uncertainty when the surface aluminum layer is oxidized. In addition, the polymer film thickness was far removed from ultra-thin (sub 100 nm) dimensions.

The average through-plane sound speed, which is the average through-plane phonon speed, was decided by the mass density and Young's modulus in a continuum solid medium; however, when approaching ultra-thin thickness scale, the PMMA films on native oxide of silicon substrate were found or expected to have a change for both mass density and Young's modulus. While undergoing changes in ultra-thin thickness, the glass transition temperature for polymeric films provided evidence for the variation in the mobility of the polymer chains, which were dependent on the dimension of the film and the substrate. These facts show that the microstructure of PMMA films differs with film substrate and film thickness. Experimental measurements for thermal conductivity of PMMA films were performed based on the assumption that the mass density and specific heat of PMMA film remained constant independent of thickness since the amount of change was quantitatively very small.

CHAPTER III

EXPERIMENTAL PROGRAM

3.1 Introduction

In this chapter, mechanical and thermal properties of selected materials are presented and the fabrication process of PMMA film is described in the sample preparation section. The succeeding section explains the methodology of TTR system for thermal property measurements and illustrates the schematic of the TTR thin-film measuring system developed in the Nanoscale Electro-Thermal Laboratory (NETSL) at Southern Methodist University (SMU). Finally, the experimental procedure to carry out the measurement of through-plane intrinsic thermal conductivity for thin PMMA films is shown, and then the experimental process and work is summarized. The fabrication of the samples was completed using apparatus of the Materials Characterization Facility (MCF) laboratory and Microscopy and Imaging Center (MIC) at Texas A&M University - College Station (TAMU), and measurement of thermal conductivity was performed using TTR system in the NETSL at SMU.

3.2 Sample Preparation

3.2.1 Material Selection/Substrate Selection

PMMA solution

PMMA is a versatile polymeric material that is well suited for many imaging and non-imaging microelectronic applications as a high-resolution positive resist for direct

writing by e-beam as well as by x-ray and deep UV micro-lithographic processes. It is also used as a protective coating for wafer thinning, as a bonding adhesive and as a sacrificial layer.

The structure of PMMA, shown in Fig. 3.1, illustrates the structure of PMMA that is due to free radical vinyl polymerization from the monomer that is methyl methacrylate. Six and eleven percent concentration of commercial 495,000 (MW) PMMA in anisole solvent and a 99.9% anisole solvent were purchased from commercial vendors. The Glass Transition Temperature (T_g) of the PMMA film was reported to be 95 $°C$ – 106 $°C$ by commercial vendor and the melting point of the PMMA film was around 150 $°C$ [23]. In order to control the thickness of the film, other concentrations of PMMA solutions (1%, 2%, 3%, 4%, 5%, 7%, 8%, 9%, and 10%) were made by mixing the two solutions and the anisole thinner. The volumes of contents for the new concentration of solutions were calculated as follows:

$$V_1 \times Con_{V1} + V_2 \times Con_{V2} = Con_{V3} \times (V_1 + V_2) \tag{3.1}$$

where V_1 and V_2 are the two volumes among the 6%, 11% solutions, and anisole thinner and Con_{V1} and Con_{V2} are the concentrations of PMMA in V_1 and V_2 respectively. Finally, Con_{V3} is the desired concentration of PMMA solution expressed by V_3, which is the sum of V_1 and V_2. Table 3.1 shows each concentration of PMMA solution and the volume of contents of the mixed solutions. The purpose of the various concentrations of the PMMA

solutions was to fabricate the various thicknesses of PMMA film at a constant spin speed.

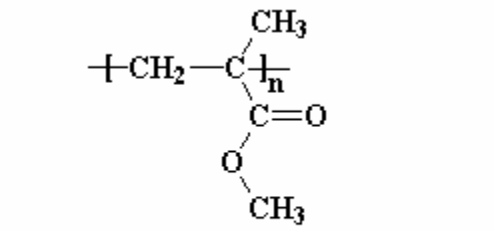

Poly(methyl methacrylate) (PMMA)

Fig. 3.1 Structures of Poly(methylmethacrylate) (PMMA)

Table 3.1 Volumetric ratio of each concentration PMMA solution

Concentration (%)	1%	2%	3%	4%	5%	7%	8%	9%	10%
11% PMMA Solution (ml)	10	20	18	28	–	10	20	15	20
6% PMMA Solution (ml)	–	–	–	–	40	40	30	10	5
Anisole (ml)	100	90	48	49	8	–	–	–	–
Mixed Solution (ml)	110	110	66	77	48	50	50	25	25

Silicon substrate

For the substrate, one side of a polished silicon wafer that was 76.2 mm (±0.5 mm) in diameter, 320 μm (±30 μm) thick, and with an orientation of (100) with ±0.5 degrees was chosen. The orientation of (100) allowed the silicon wafer to be split easily with a diamond cutter. In order to avoid any scratches on the substrate, the cutting procedure should be performed by touching the surface as little as possible. The silicon wafer had a native oxide layer on the surface and the oxide layer played a role of adhesives between PMMA and substrate.

3.2.2 Fabrication of PMMA Films with Varying Film Thickness

Prior to the application of the film, all of the silicon wafers were cut into 2×2 cm as shown in Fig. 3.2, cleaned in an ultrasonic cleaning device using acetone, and then rinsed with isopropanol. Substrate cleaning was accomplished by using a Reactive Ion Etcher (R.I.E.), Mach Plasma System Model CS-1701, as shown in Fig. 3.3. This plasma reacts with organic molecules but does not affect silicon, silicon oxide, silicon nitride, or metal surfaces. On the other hand, the silicon oxide causes PMMA film to attach firmly to the substrate, so this plasma treatment should be the last step of the cleaning procedure. Oxygen, O_2, plasma with 200 W power was finally used on each cut silicon wafer for 300 seconds as a last cleaning procedure to remove any lingering organic molecules. Actual parameters for the RIE process are shown in Table 3.2.

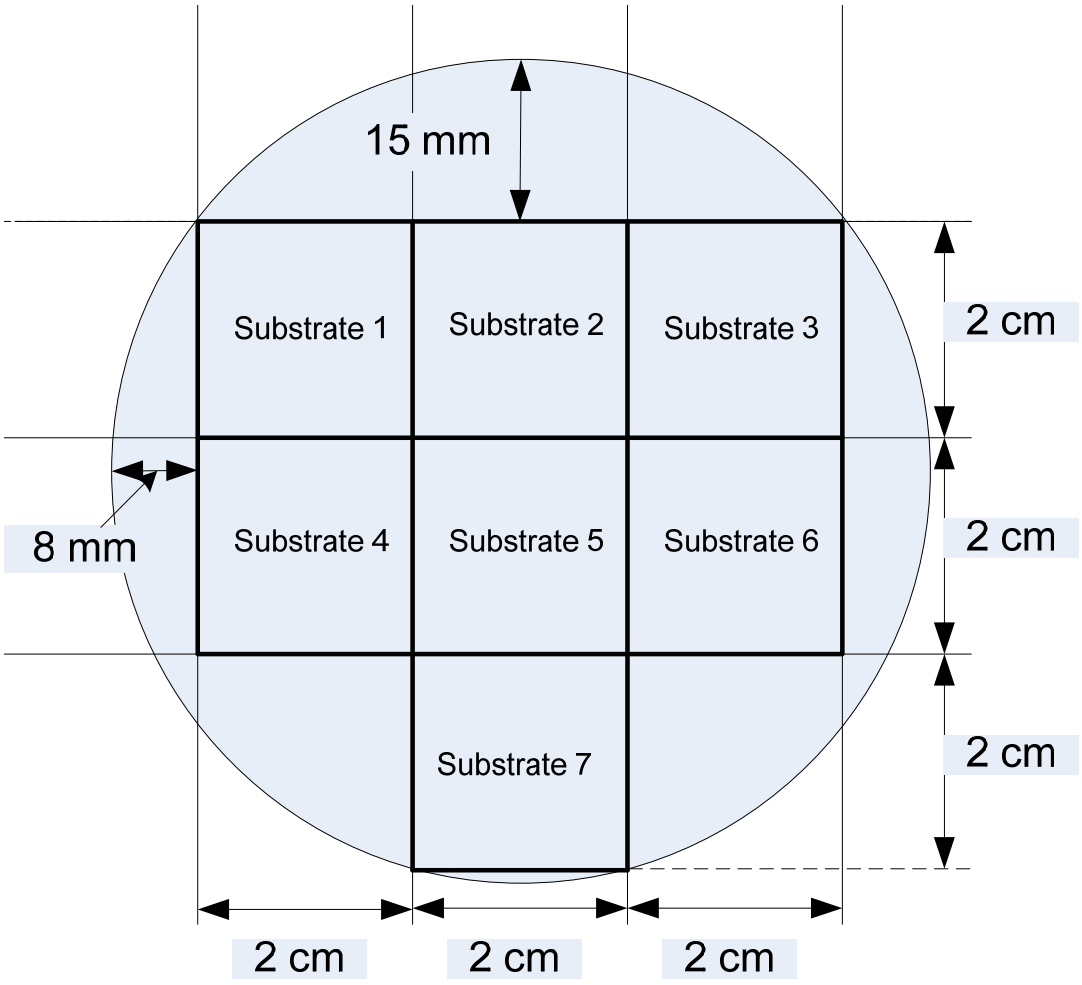

Fig. 3.2 Schematic of silicon wafer for seven substrates; each cut substrate is 2×2 cm

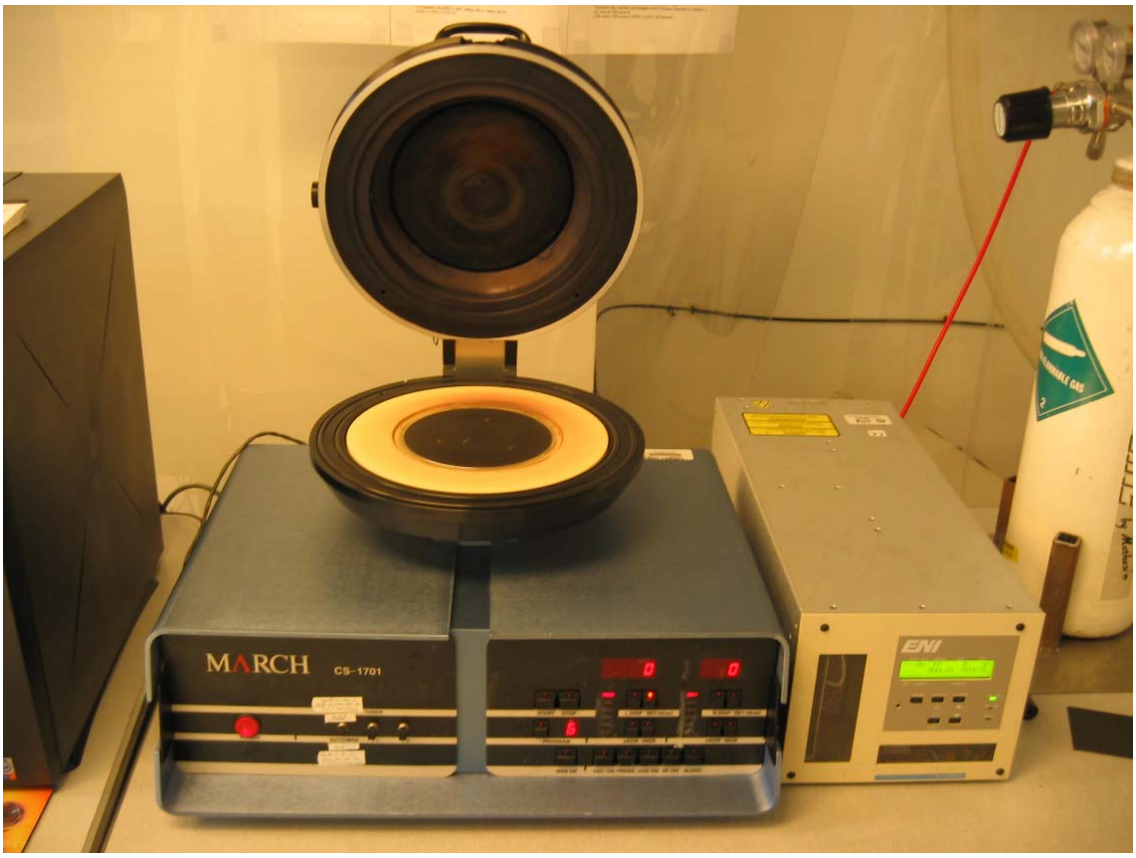

Fig. 3.3 March Plasma Systems Model CS-1701 reactive ion etcher in the MCF Laboratory

Table 3.2 Actual properties of RIE during the O_2 plasma running time for cleaning 2×2 cm silicon substrate

Pressure (mTorr)	Power (Watts)	Time (sec.)	Temp (˚C)	Percentage of MFC opening	MFC* size	Conversion Factor for O_2	O_2 Gas Flow
290	204	300	5	20 %	250 sccm	0.994	49.7 sccm

* Mass Flow Controllers with its orifice size in Standard Cubic Centimeters (SCCM).

In this study, thin films were deposited by spin coating solutions of the polymer in anisole onto a native oxide of silicon wafer. The percent concentrations of solid of PMMA in anisole solvent ranged between 1% to 11% and were used to spin-coat a range of film thicknesses from 2.02 μm to 40 nm on to the substrates. In order to reduce film non-uniformity and the number of parameters, the spin coater speed for each sample was kept at 3000 rpm for all PMMA concentrations used except for 1.31 and 2.02 μm films, which were spun at 2100 rpm and 1200 rpm, respectively, with an 11% solution concentration. PMMA films were fabricated by using the SCS P6204 (8-in. bowl) non-programmable Spin Coater, as shown in Fig. 3.4.

The dwell spin time was held constant at 45 seconds and room temperature was maintained followed by a soft-bake of the coated PMMA films on a preheated hotplate at 180°C for 85 seconds. This later step ensured complete evaporation of the anisole solvent from the PMMA film after spin coating. There are two kinds of baking methods for PMMA film: a hotplate and a convection oven for baking. The hotplate conducts heat from the bottom of the substrate to the top of the coated PMMA film, while the oven conducts heat from the outside of the sample to the inside. Baking a substrate from the "outside in" such as occurs with the oven creates a skin on the surface of the film, similar to an ice bound pond, thus trapping solvent since heat is applied to the outer surface of the film first. This trapped solvent forms blisters or bubbles in the film. Using the hotplate does not cause skin formation during solvent evaporation since hotplate baking heats the substrate from the bottom up. Therefore, soft contact baking by hotplate was used as the baking method in this experiment.

Fig. 3.4 The SCS P6204 (8-in. bowl) non-programmable spin coater in the MCF Laboratory

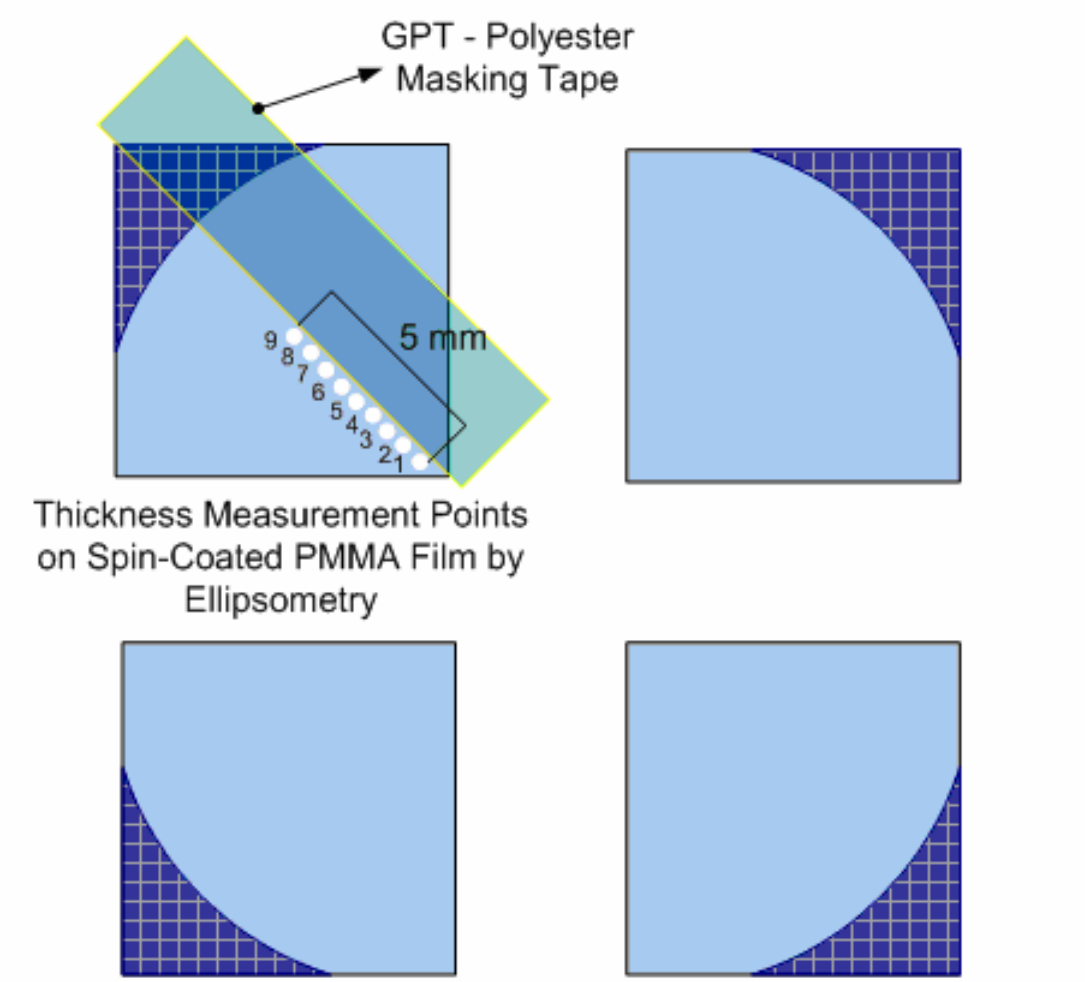

Fig. 3.5 Schematic of sample that was covered by masking tape after cutting spin-coated sample to 4 pieces

After spin-coating the PMMA film onto the 2×2 cm silicon wafer, each sample was divided into four pieces, and a small area of one of the four pieces was covered with polyester masking tape as shown in Fig. 3.5. This shadow mask technique creates a cross-sectional step in the gold (Au) layer when it was deposited by sputtering. The tape ensures that a cross-sectional step exists so that the Dektak^{3}ST profilometer could be employed correctly for thickness measurement of the deposited gold layer. The nine white points are the number and the location of the thickness measurement for the film.

Finally, thickness measurements for the spin-coated films were taken in the area of the applied masking tape using a Gartner Stokes Ellipsometer that is an apparatus of the NETSL at SMU before the gold was deposited. The measured thicknesses of each sample ranged from bulk (2.02 μm) to ultra-thin (40 nm). Details are described in the result and discussion section.

3.2.3 Gold (Au) Deposition on PMMA Films by Sputtering Method

In order to use the TTR method, heat must be absorbed from the pump laser into the deposited metal layer that lies on top of the transparent spin-coated PMMA film. According to Burzo et al.[22,24,25], the thickness of the metal layer and its material properties significantly impacts the responsivity of the TTR procedure; therefore, extreme care must be taken to control its thickness and the rate of deposit onto the PMMA film.

A gold layer was chosen as the absorption layer because of its high absorptivity, reflectivity, high thermo-reflectance coefficient, and low oxidation as presented by

Mihai G. Burzo and Pavel L. Komarov[24]. Moreover, its optical properties are well known when used with the TTR method. However, the thickness of the heat absorbing Au layer must be carefully chosen so that the optimum responsivity and the minimum uncertainty can be obtained from the TTR setup. Thus, the thickness of the Au layer to be deposited was chosen beforehand to maximize the responsivity of the TTR measurement.

A pure gold layer (99.99%) was deposited via a sputtering method directly onto a cleaned silicon wafer and 13 spin-coated PMMA films with 40 mA current using a Sputter Coater 208HR (Fig. 3.6) in the Microscopy and Imaging Center (MIC) at Texas A&M University prior to the measurement of thermal conductivity. However, the ρC_p of the Au layers may have different values depending on the deposition technique. Therefore, an Au layer was sputter-coated on a silicon wafer during the sputter-deposition simultaneously with the PMMA film samples. The sample, consisting of an Au layer, native oxide, and a silicon wafer, was used for the ρC_p measurement of the Au layer with the TTR method.

Fig. 3.6 Sputter Coater 208HR in the Microscopy and Imaging Center (MIC)

The proper thickness of the Au layer required is approximately 500 nm onto the PMMA film; however, the dimensions of the gold target were not enough to provide the proper thickness with the Sputter Coater 208HR. This problem was solved by reducing the distance between the gold target and the samples using a petridish as shown in Fig. 3.7. The petridish played the role of an alternative sample stage with the original sample stage with the open end facing down in order to increase the stage height. The PMMA film samples were situated on the petridish inside the border.

This approach increased the Au thickness on the PMMA films, but it made thickness measurement difficult because of the discrepancy between the axis of the gold target disk and the axis of the petridish as shown in Fig. 3.7. The sputter employs a crystal head for thickness monitoring, and the location of the crystal head hampered the identification of the two axes.

The thickness measurements for the Au layer at different locations within each sample showed slight variations as well as variations in the average thickness for the Au layer from sample to sample. The reason is that the central axis of the gold target was not equal to the one of circularly arranged samples and the small gold target could not cover the large area of the samples because the diameter of the gold target disk was smaller than the diameter of the circularly arranged samples.

However, this issue was solved by constricting the locations of all measurements as follows:

$$\{A_{PMMA,\,h}\} \supseteq \{A_{gold,\,h}\} \supseteq \{A_{PMMA,\,K}\} \tag{3.2}$$

where $A_{PMMA,\,h}$ is the thickness measurement area of the PMMA film, $A_{gold,h}$ is the thickness measurement area of the deposited gold layer, and $A_{PMMA,K}$ is the thermal conductivity measurement area in a sample.

A Dektak^{3}ST profilometer was employed to measure the thickness of the sputter-coated Au layers on PMMA films by using the created step created by the shadow mask technique. Finally, thirteen samples, with PMMA films with various thicknesses under the Au layer, were prepared along with one Au layer/silicon wafer sample for ρC_p measurement of the Au layer. A schematic of a typical sample is shown in Fig. 3.8. The measured thickness data for the PMMA films and Au layers are presented in the result section.

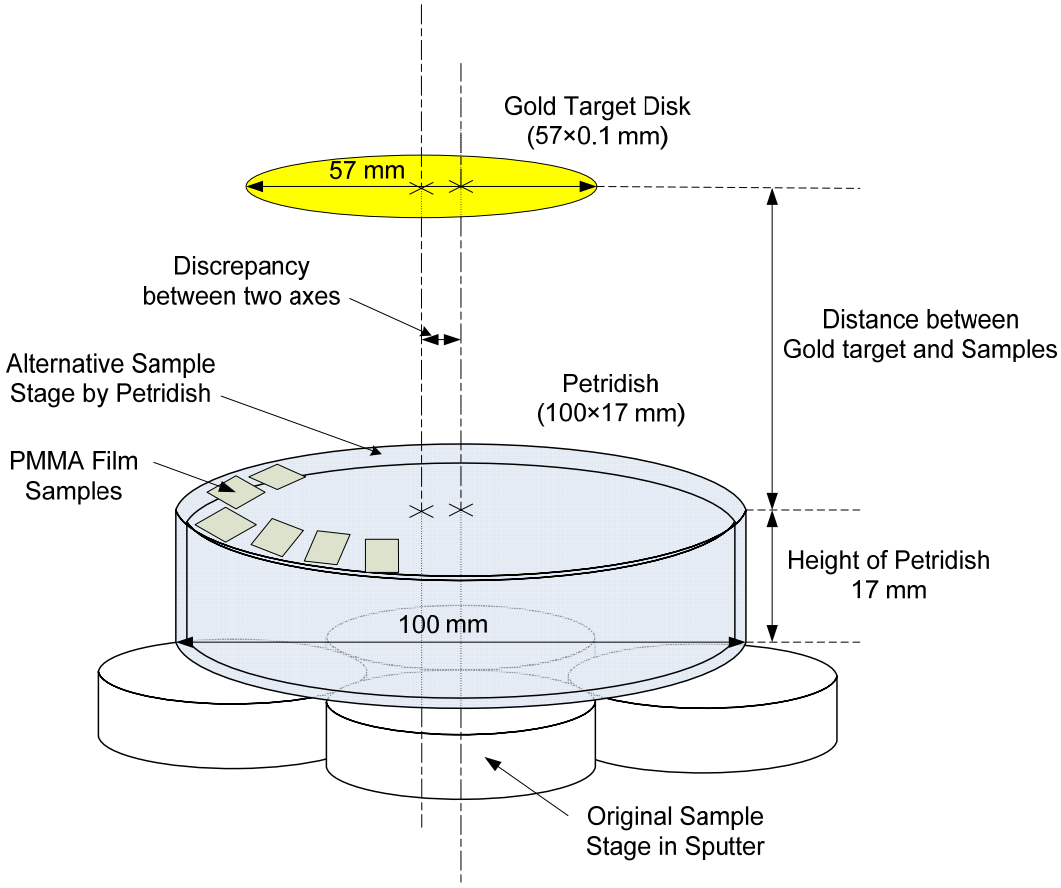

Fig. 3.7 Schematic inside a sputter chamber, which shows samples on alternative sample stage by petridish

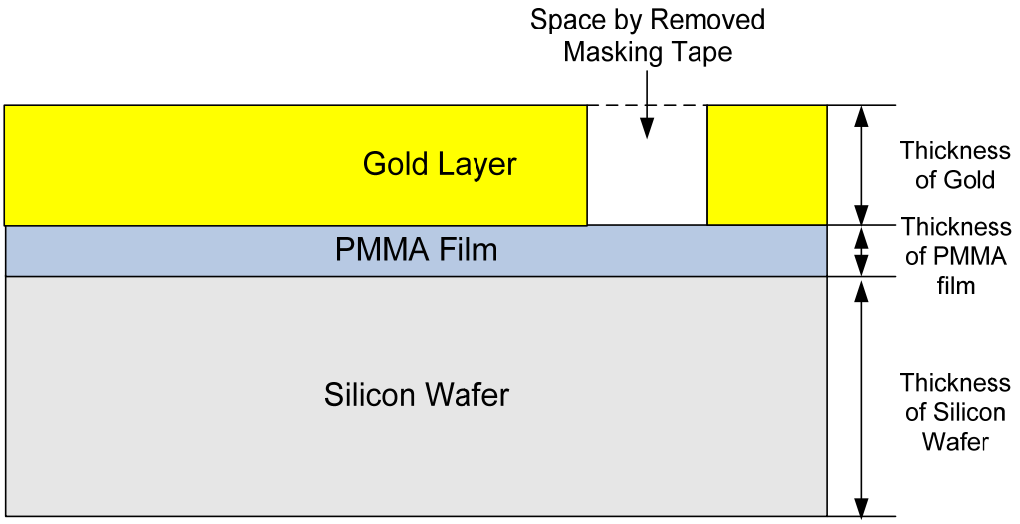

Fig. 3.8 Schematic of a cross section after removal of masking tape in a gold-deposited sample

3.3 Measurement of Thermal Conductivity by the Transient Thermo-Reflectance (TTR) Method

3.3.1 Transient Thermo-Reflectance (TTR) Measurement Methodology

The TTR measurement for through-plane thermal conductivity of thin PMMA film was performed using a new compact TTR system developed in the NETSL at SMU. The basic principle of the transient thermal reflectance method is to heat a sample by laser irradiation and probe the changes in the surface reflectivity of the heated material. The source of energy in the TTR method is normally provided by a pulsed laser with short pulse duration. During each pulse, a given volume below the sample surface heats up due to the absorbed laser light energy. The depth of the volumetric heating is determined by the optical penetration depth, which is a function of laser wavelength and surface material properties. After each laser pulse, the sample cools down to the initial ambient temperature. During this process, a probing CW laser light reflected from the sample surface at the heating spot center is collected on a photodetector (1 ns maximum rise time) that reads the instantaneous surface reflectivity, as shown in Fig. 3.9.

The TTR system uses the fact that the relative change in the temperature of the surface material is linearly proportional with the relative change in the reflectivity within a wide but finite temperature range:

$$\frac{\Delta T}{T} = \frac{\Delta R}{R} \tag{3.3}$$

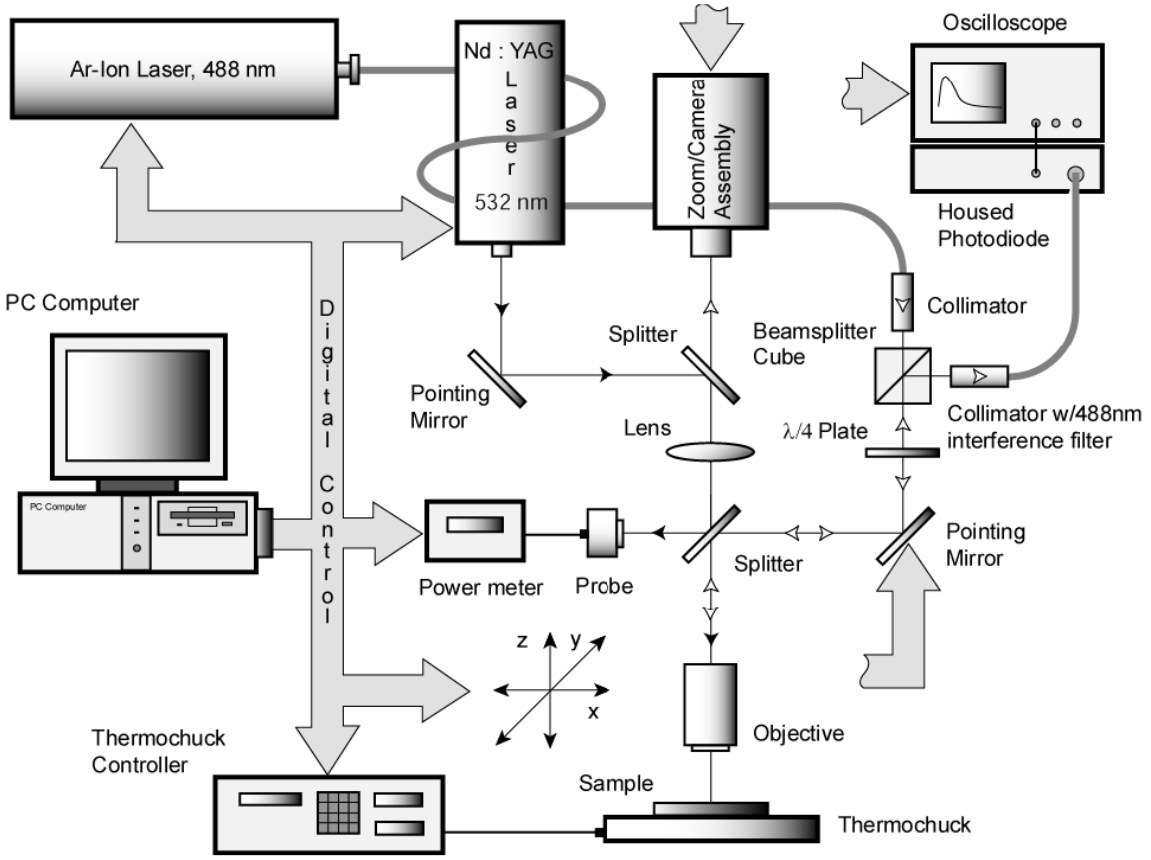

Fig. 3.9 Schematic of the Transient Thermo-Reflectance (TTR) system in NETSL at SMU by Burzo et al.[22]

where T is the temperature and R is the reflectivity of the materials. The changes in surface reflectivity, are then recorded by an oscilloscope (at rates of up to 5 GS). The above-mentioned principle has been experimentally and analytically proven by Qiu and Tien[26,27], Burzo et al.[22,24,25] and Komarov et al.[25].

The result of the experiment is a transient normalized temperature response, which represents the overall heat transfer behavior of the layers of materials including the unknown material under test. To extract the thermal conductivity from the recorded temperature response, an identical mathematical representation of the corresponding physical measurement problem is solved numerically with guessed thermal properties with the intention of matching the experimental and numerical transient normalized temperature responses. A mathematical optimization technique makes it possible to systematically vary the desired unknown properties and compare each resulting numerically-obtained response to the reference experimental data until the error between them is minimized in the RMS sense. The final numerical solution hence yields the desired unknown parameters, which represent the best fit to the actual thermal properties of the physical sample.

By using a two-parameter optimization technique, the method described in this work yields not only the thermal conductivity of the material under test but also the interface resistance between this material and the absorption layer on top of it. The transient heat transfer in the TTR method can be described by the use of the heat equation, as follows:

$$\rho C_p\left(\frac{\partial T}{\partial t}\right) = \nabla(K\nabla T) + \dot{Q}_{ab} \tag{3.4}$$

where ρ is the mass density of the material, C_p is its specific heat, t is the time, K is its thermal conductivity, and $\dot{Q}_{ab}$ is the heat source created by absorption of the laser light energy. The TTR system developed by the NETSL was designed to perform through-plane only or both through-plane and in-plane thermal properties measurements. In order to be able to measure both the through-plane and in-plane thermal properties the two-dimensional heat transfer is used. In this case, the heat transfer inside the sample under test is governed by the 2D heat equation in polar coordinates and can be written as follows:

$$\left(\frac{\partial T}{\partial t}\right) = \alpha(T)\left(\frac{\partial^2 T}{\partial r^2} + \frac{1}{r}\frac{\partial T}{\partial r} + \frac{\partial^2 T}{\partial z^2}\right) + \frac{1}{\rho C_p}\dot{Q}(r,z,t) \tag{3.5}$$

where r and z are dimensionless coordinates and α is the thermal diffusivity of the material, which is $\alpha = K/(\rho C_p)$. The heat source, $\dot{Q}$, was introduced as follows:

$$\dot{Q}_{(r,z,t)} = I(t)(1-R)\gamma e^{-\gamma z} \tag{3.6}$$

where γ is the absorption coefficient of the top layer, and $I(t)$ is a Gaussian temporal distribution as follows:

$$I(t) = \frac{2F}{\tau\sqrt{\pi}} e^{-4\left(\frac{t-t_0}{\tau}\right)^2} \tag{3.7}$$

where F is the fluence of laser irradiation, τ is the duration of the heating laser pulse which is 6.1 ns, and t_0 = 7 ns is the time at which the intensity reaches its maximum value.

In this study, the one-dimensional TTR measuring approach can be used, since the purpose of this study was to measure the through-plane thermal conductivity of PMMA film. It is worth mentioning that the dimension of the probing spot is close to two orders of magnitude smaller than the heating laser spot, thus assuring the applicability of the one-dimensional approach. As a result, the heated sample under test can be treated as a semi-infinite solid for the one-dimensional problem. The diameter of the heated spot (YAG Laser) is 185 μm, while the probing spot is around 2.5 μm, which is small enough to make $\frac{\partial T}{\partial r} \approx 0$ in the probing spot area. Thus, the one-dimensional heat equation is induced from the 2D Eq. (3.5) as follows:

$$\left(\frac{\partial T}{\partial t}\right) = \alpha\left(\frac{\partial^2 T}{\partial z^2}\right) + \frac{1}{\rho C_p}\dot{Q}_{ab}(z,t) \tag{3.8}$$

The first boundary condition is an adiabatic boundary condition at the top of the sample as follows:

$$\left(\frac{\partial T}{\partial t}\right) = 0 \text{ , at } z = 0 \tag{3.9}$$

since the time scale of the TTR is in the nanosecond range, natural convection and conduction from the sample to the surrounding medium (air) can be neglected.

The second boundary condition is an isothermal boundary condition at the bottom of the sample as follows:

$$T = T_{chuck} \text{ , at } z = \infty \tag{3.10}$$

because the sample is located on a thermo-chuck that keeps the temperature constant at T_{chuck}. Initially, since the materials are at ambient temperature, the initial condition is written as follows:

$$T = T_{ambient} \text{ , at } t = 0 \tag{3.11}$$

During the heating and cooling process, the instantaneous surface reflectivity is acquired by the probing CW laser light reflected from the sample surface at the center of the heated spot, and then the thermal diffusivity of the material is extracted by solving the one-dimensional inverse heat Eq. (3.8) based on Eq. (3.3) as shown by Burzo et al.[25]. This was accomplished by first numerically simulating the transient heating

caused by the laser pulse and then fitting the experimental results with the computed data in the TTR system.

3.3.2 Transient Thermo-Reflectance (TTR) Measurement

Figure 3.10 depicts schematically the heating and probing beams used by the Transient Thermo-Reflectance system and also shows the sample under test. In the system built in the NETSL at SMU, the heating source is an Nd: YAG laser, that is pulsed at 30 Hz with a wavelength of 532 nm, a maximum output pulse energy of 0.5 mJ/pulse, and a pulse-width of 6.1 ns. The probing light source is a CW Ar-Ion laser with a wavelength of 488 nm in a single-mode irradiation and maximum output of 25 mW. The amount of heating energy used from the heating source was 25.71 μJ/pulse which was measured directly by a power meter and the fluence was 957 J m^{-2} for the samples measured.

Once the transient TTR temperature response was obtained from measuring the relative change in the reflectivity of the samples the data was fitted with the numerically obtained transient temperature signal. The numerical simulation of the transient temperature response was computed from the solution of the heat equation by using the thermo-physical properties of the materials composing the samples. Table 3.3 summarizes the material properties utilized to measure the intrinsic thermal conductivity of each PMMA film sample.

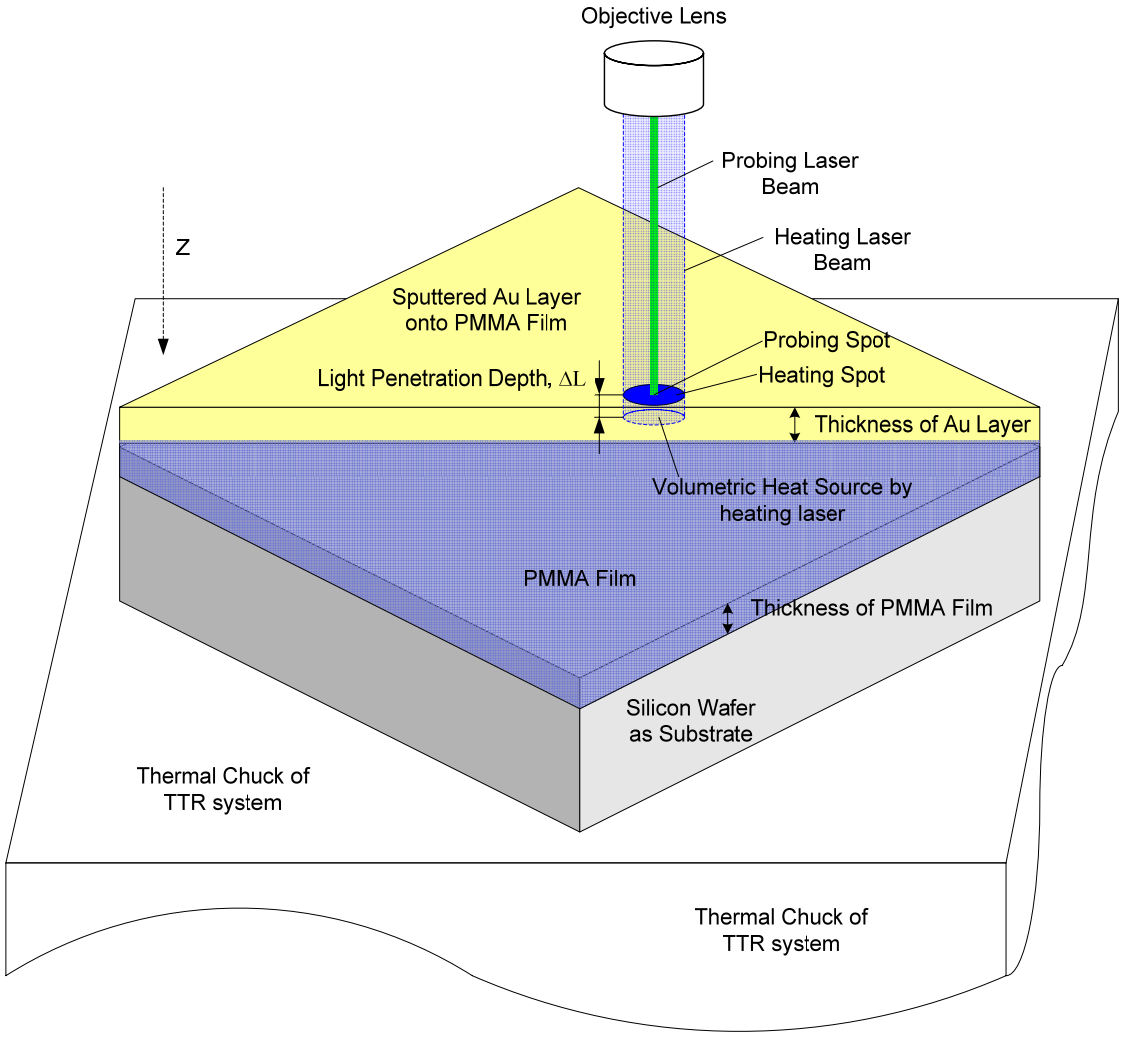

Fig. 3.10 Schematic of heating and probing spots on the Au layer that was sputtered onto the PMMA film sample

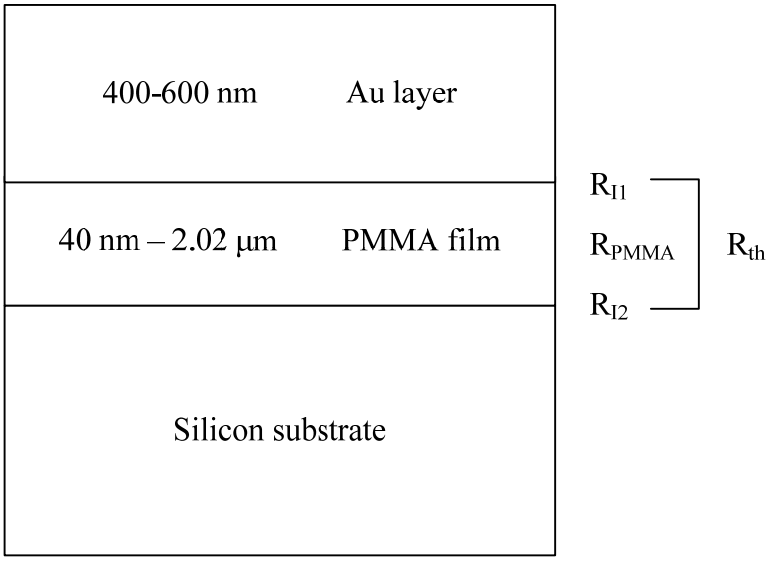

Fig. 3.11 Schematic of samples that consist of Au layer, PMMA film, and silicon substrate with total thermal resistance (R_{th}) and interface thermal resistances (R_{I1}) between Au layer and PMMA film, and (R_{I2}) between PMMA film and silicon substrate: $R_{th} = R_{I1} + R_{PMMA} + R_{I2}$

Table 3.3 Properties of the samples utilized in the TTR system

Materials	ρCp ($Jm^{-3}K^{-1}$)	K ($Wm^{-1}K^{-1}$)	n	k	h (Å)	R_I (10^{-8} m^2KW^{-1})
Si Substrate	1.65×10^6	150	–	–	3,200,000	negligible
PMMA Film	1.75×10^6	unknown***	–	–	measured data*	0.5 (R_{I2})
Au Layer	2.19×10^6	315	0.467	2.45	measured data**	unknown (R_{I1})***

* measured film thickness by Gaertner Stokes Ellipsometer
** measured gold layer thickness by Dektak^{3}ST profiler
*** value that will be measured by TTR system

The TTR method can evaluate at most two unknown properties. The thickness of each layer making up the samples was measured by either an ellipsometer or a profiler, as mentioned previously. The interface thermal resistance R_{I2} between the PMMA film and the silicon wafer was measured by applying the TTR method to the samples that had "bulk" thickness.

There are two interface thermal resistances in the sample as depicted in Fig. 3.11. Since the interface thermal resistance, R_{I2}, between the PMMA film and the silicon substrate was independent of the PMMA film thickness and had good adhesion to the native oxide of the silicon wafer, the R_{I2} value was assumed to be constant for all samples. In order to measure the interface thermal resistance, R_{I2}, the two unknown parameters were the interface thermal resistance R_{I1} between the Au layer and PMMA film and the thermal conductivity of the bulk PMMA film. These were measured by the TTR method using samples A11-002, A11-023, and A11-102 which assumed an intrinsic thermal conductivity for the bulk PMMA film as 0.19 W m^{-1} K^{-1} as shown in Table 3.4. The measured R_{I2} was 0.5×10^{-8} m^2 K W^{-1} in the bulk PMMA film samples; however, it was also confirmed that the effect of R_{I2} on thermal conductivity was less than 1% in all samples. In addition, the measured value for R_{I2} includes the thermal resistance of the native oxide layer.

The mass density and specific heat of silicon, PMMA, and gold are well known in bulk dimensions. However, since the Au absorption layer was not in bulk, it was expected that its thermal capacitance varied when compared to the bulk value. Specifically, the ρC_p of Au layer was determined independently using the specially

prepared Au film on the silicon substrate sample. The measurement results are shown in Table 3.5 with the measured average ρCp for the Au layer equal to 2.19×10^{6} J m^{-3} K^{-1}. The obtained value was then utilized for all TTR measurements for all the samples considered in this work.

Table 3.4 Utilized properties of the samples to measure interface thermal resistance, R_{I2} in TTR method by using the bulk thick PMMA films (sample #A11-102, A11-023, A11-002)

Materials	ρC_p (Jm^{-3} K^{-1})	K ($Wm^{-1}K^{-1}$)	n	k	h (Å)	R_I (10^{-8} m^2KW^{-1})
Si Substrate	1.65×10^6	150	–	–	3200000	negligible
PMMA Film	1.75×10^6	0.19	–	–	10206; 13102; 20207	unknown R_{I2}
Au Layer	2.19×10^6	315	0.467	2.45	5084; 5538; 5957	unknown R_{I1}

Table 3.5 Measured ρCp of Au layer and material properties utilized in TTR method

Material	ρCp ($Jm^{-3}K^{-1}$)	K ($Wm^{-1}K^{-1}$)	n	k	h (Å)
Si	1.65×10^{6}	150	-1	-1	3200000
Thick-Au layer	2.21×10^{6}	315	0.467	2.45	5144
Thin-Au layer	2.14×10^{6}	315	0.467	2.45	4208
Average value in Au Layer	2.19×10^{6}	315	0.467	2.45	–

Using the above properties for the Au layer, the light penetration depth, (Δ_L), and heat propagation depth, δ_H, were calculated as follows:

$$\Delta_L = \frac{\lambda}{4\pi k} \tag{3.12}$$

$$\delta_H = (\alpha\tau)^{\frac{1}{2}} \tag{3.13}$$

where λ is the wavelength of the laser, δ_H is the heat propagation depth during the heating pulse, and τ is the pulse width of the heating laser. Thus, the light penetration depth and the heat penetration depth can be compared with the thickness of the top Au layer, which is the absorption layer for the heating laser. The calculated penetration depth for the heating caused by the pulsed laser light was calculated as 17.3 nm for the deposited Au layer.

According to a previous work by Burzo et al.[24] and Komarov, P.L. and Raad, P.E.[28], the heat penetration depth in the absorption layer should be comparable to the specified layer thickness range as defined by the nondimensional thickness, H:

$$H = \frac{h}{\sqrt{\alpha\tau}} = \frac{h}{\delta_H} = \frac{1}{\sqrt{Fo}} \tag{3.14}$$

where Fo is the Fourier number defined as $Fo=\alpha\tau/h^2$. In a previous work the terms "thermally thin", "thermally thick", and transition regime, were defined and it was shown that the responsivity of the TTR measurements for measuring the thermal conductivity of the underlying bulk silicon dioxide ($K \approx 1.4$ W m^{-1} K^{-1}) and bulk silicon sample ($K \approx 150$ W m^{-1} K^{-1}) is sufficiently high within the thickness of the absorption layer that is the transition regime ($0.4 \leq H \leq 2$), and more widely, in the regime ($0.1 \leq H \leq 2$).

However, when a heating laser energy that corresponds to a fluence of 207 J m^{-2} was applied on a 90 nm (H ≈ 0.1) thick layer of Au that was deposited on a 320 nm PMMA film, a deterioration of the absorption layer was observed possibly due to melting or high temperature gradients at the interface between the Au and PMMA layer. On the other hand, thicker layers ($H \geq 2$) would hide the influence of thermal properties of any underlying material. As results, it was chosen to deposit Au layers with thickness ranging between 400 nm and 600 nm onto the PMMA films.

Table 3.6 shows the thermal and optical properties for the Au layer of samples. The actual thickness of the deposited Au film, h, was within the intervals $\Delta_L << h < \delta_H$ and $0.43 \leq H \leq 0.64$. Although the thermal conductivity of PMMA film was less than that of silicon dioxide by approximately one order of magnitude, the nondimensional thickness of Au layer in the range $0.43 \leq H \leq 0.64$ corresponds to a sufficiently high responsivity for measuring the thermal conductivity of the embedded PMMA films.

The thermal conductivity was measured at three different locations in the immediate vicinity of the area measured for the gold thickness, and was measured twenty times at each position. Each of the twenty measurements in a given position consisted of 500 shots using the heating laser and each TTR measurement was performed using the probing laser for a single heating shot.

Table 3.6 Thermal and optical properties of the Au layer deposited on PMMA films

material	K ($Wm^{-1}K^{-1}$)	ρC_p ($Jm^{-3}K^{-1}$)	α (m^2s^{-1})	k	h (nm)	Δ_L (nm)	δ_H (nm)
Au	315	2.19×10^{6}	1.44×10^{-4}	2.45	400 – 600	17.3	940

On the other hand, each of the twenty averaged values in a position was an average of 500 TTR measurements. Thus, one position had a total of twenty average values for the 20×500 heating shots in the TTR measurement. The dimensions for the heating and probing spot, using a 20× objective lens, (YAG Laser) were 185 μm and 2.5 μm, respectively, thus the ratio of spot diameters was 74. This value ensures that the 1-D heat equation, Eq. (3.8), assumption can be used instead of the 2-D expression, Eq. (3.5).

Finally, the samples, which consisted of an Au layer and PMMA film deposited on the native oxide silicon wafers, were tested using the TTR experimental system. These measurements used the unknown parameters, namely, the intrinsic thermal conductivity, K, of the PMMA film and an interface thermal resistance, $R_{I1,}$ between the Au layer and the PMMA film that were measured previously.

3.4 Summary of Experimental Process/Work

In this study, the experimental procedure can be divided to three steps: step 1 is a sample preparation for ultra-thin and thin PMMA films, step 2 is a sample preparation to apply the TTR method, and step 3 is performing the TTR measurement for thermal conductivity of the prepared samples. Each step was depicted as a flow-chart diagram in Fig. 3.12.

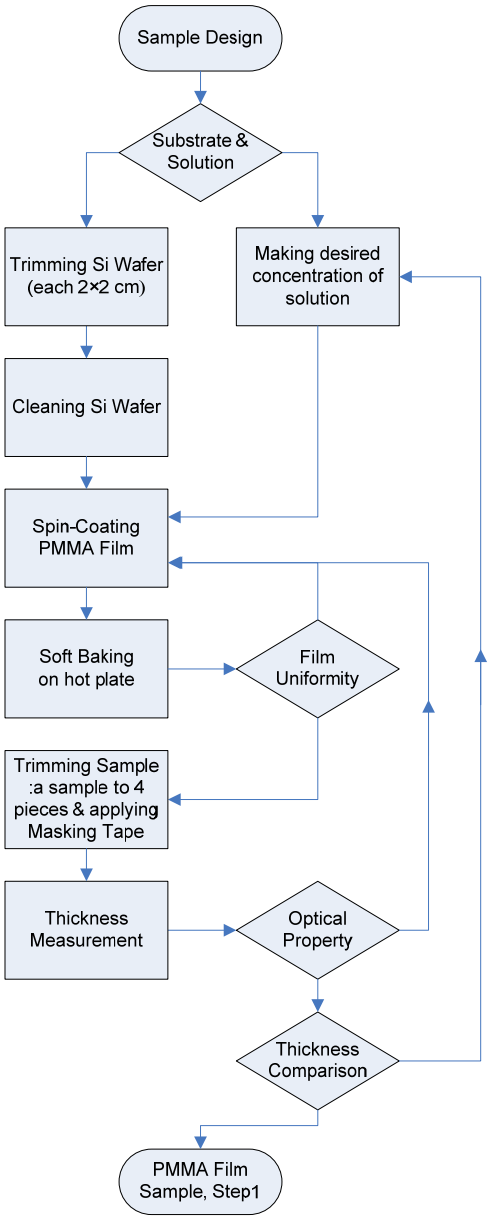

Sample Preparation,
Step 1

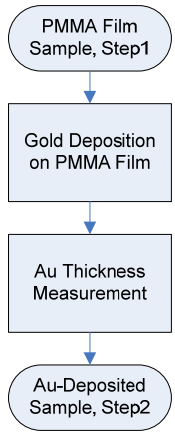

Sample Preparation,
Step 2

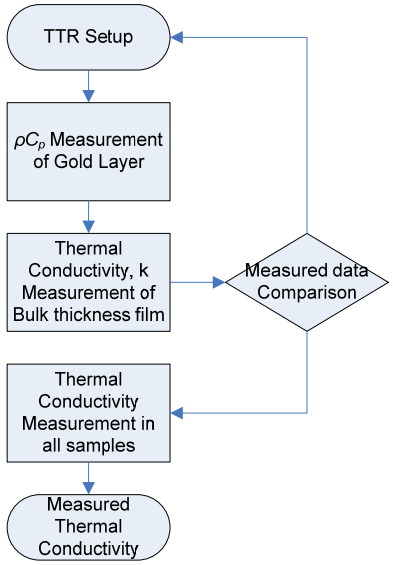

Thermal Conductivity
Measurement by TTR sys.
Step 3

Fig.3.12 Summary of sample preparation and thermal conductivity measurement procedure as flow chart

CHAPTER IV

RESULTS AND DISCUSSION

4.1 Introduction

In this chapter, the measured thickness of the samples is presented before the result of TTR measurements. Since the focus of this study was to determine the degree of dependence on film thickness for thermal conductivity, the precise measurement of thickness for the PMMA films was a priority condition for a proper sample, and the thickness of each sample was measured by ellipsometer.

It is clear that the thickness of the Au layer, which is the absorption layer for the heating laser, strongly influences the performance of the TTR system. Thus, the thickness measurement of the Au layer was performed as accurately as possible by using a profiler. Finally, the TTR measurement for the PMMA films was performed within the area where the thickness of the both PMMA film and Au layer was measured, and the analyzed data are shown in this chapter.

4.2 The Measured Thicknesses of PMMA Films

The PMMA film thickness was measured in nine different locations using an ellipsometer at each measurement position of the sample. Samples were eliminated from this experiment if improper oscillation of the refractive index occurred, at even one of the nine positions in each sample, during the thickness measurement.

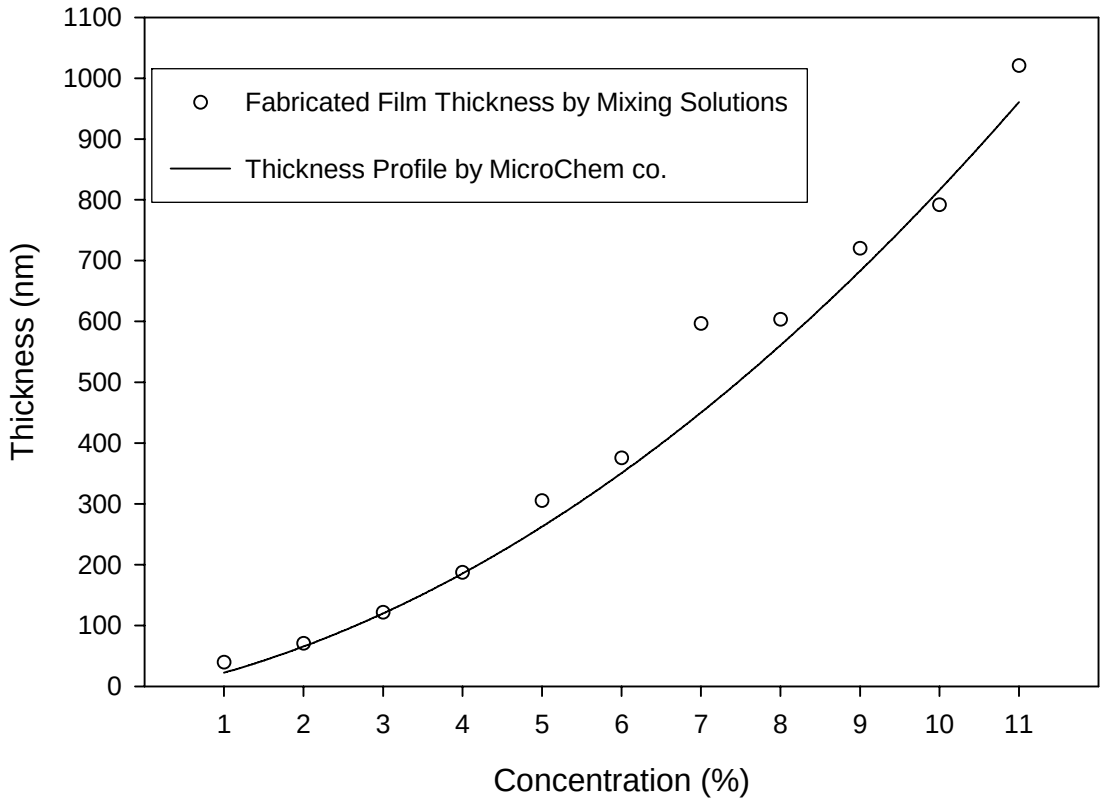

Fig. 4.1 Thickness profiles versus concentration of PMMA solution with spin-speed at 3000 rpm

The plot of thickness as a function of concentration is shown in Fig. 4.1 without the two bulk thick samples, which were spun at 2100 and 1200 rpm with 11% PMMA in anisole solvent. Most of the measured thicknesses in each sample corresponded well with the vendor's data except sample number A7, which is 7% PMMA in anisole solvent. In order to set a reference value for the thermal conductivity in bulk films, two bulk thickness samples, 1.31 and 2.02 μm, were fabricated at a spin speed of 2100 and 1200 rpm respectively, using an 11% concentration of solution. The thermal conductivities for the 1.02, 1.31, and 2.02 μm thick samples were considered bulk PMMA film values. These three bulk thickness samples were utilized as references and used to set up the TTR system.

Table 4.1 shows the measured thickness of PMMA films that were made by using the various concentrations (%) of PMMA in an anisole solvent (from samples A1-005 to A11-002) and by varying the spin speed (sample number A11-023 and A11-102). The measured thickness values for samples numbered A7-006 and A8-004 showed close thickness measurements in relation to each other, even though the concentration of the PMMA solution was different. The reason may be attributed to an error in mixing of the solutions since the concentrations of the solution were controlled by mixing 6 % and 11 % PMMA solutions; however, these samples were still used for TTR measurement. Although fluctuation of the refractive index was observed depending on film thickness, i.e. the 39.7 nm film had n = 1.36 whereas the other samples had a value n = 1.49 in the real part of the refractive index, the 39.7 nm PMMA film with n = 1.36 was accepted for TTR measurement.

Table 4.1 Measured film thickness and real part of the refractive index versus concentration of PMMA in Anisole solvent

Sample number	% PMMA in Anisole	Spin Speed (rpm)	h (nm)	σ (nm)	$W_{h,95\%}$ (%)	n
A1-005	1%	3037	39.7	0.07	0.22	1.36
A2-002	2%	3011	70.8	0.24	0.27	1.47
A3-004	3%	3021	121.7	1.03	0.62	1.49
A4-003	4%	3030	187.5	0.35	0.32	1.49
A5-004	5%	3015	305.2	0.66	0.44	1.42
A6-003	6%	3018	375.7	0.84	0.50	1.49
A7-006	7%	3030	596.6	0.22	0.28	1.49
A8-004	8%	3018	603.5	0.66	0.46	1.49
A9-004	9%	3029	720.1	3.92	2.24	1.44
A10-004	10%	3014	791.9	0.34	0.29	1.49
A11-002	11%	3024	1020.6	0.54	0.32	1.50
A11-023	11%	2123	1310.2	1.21	0.54	1.49
A11-102	11%	1213	2020.7	4.71	1.83	1.46

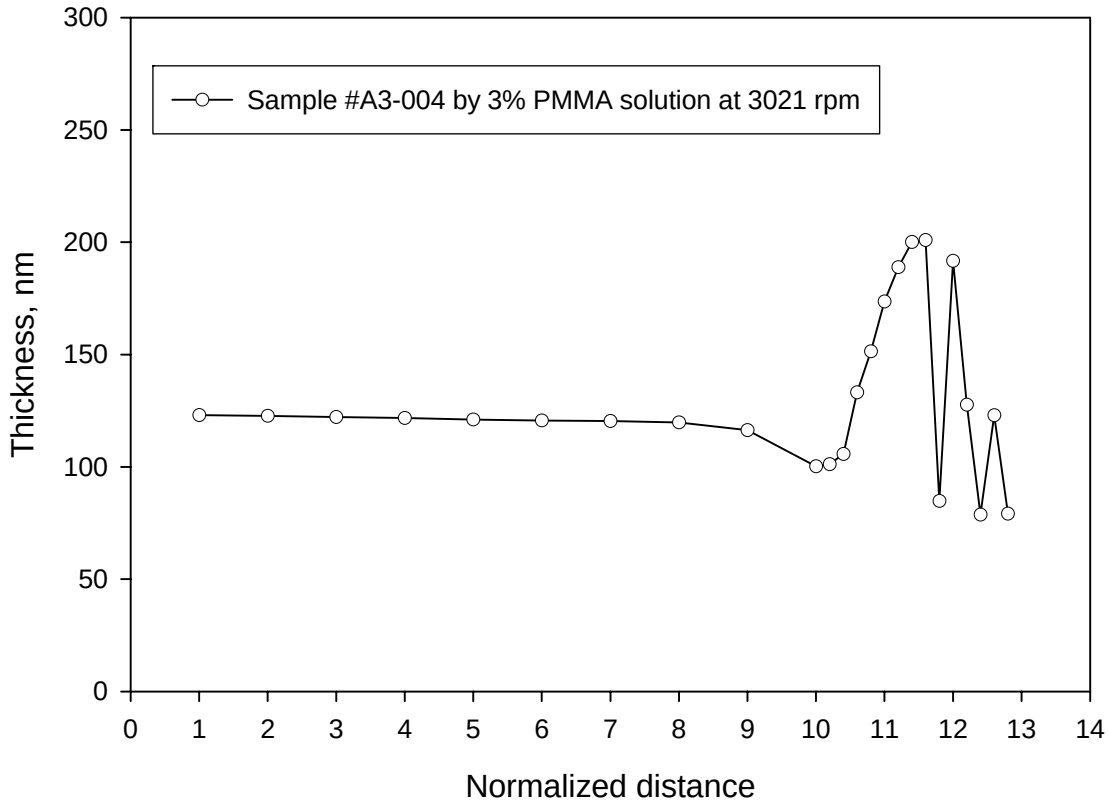

Fig. 4.2 Thickness profile versus normalized distance from near spin-axis in a surface of PMMA film

However, the thickness of the film may have had an effect on the refractive index, so a change of optical properties in the ultra-thin polymer film remains a concern. Thus, the investigation for whether or not mechanical or chemical properties are changed depending on optical properties in the ultra-thin films remains for future work. Positions for the measurement of thickness on the surface of a PMMA film were important with respect to measurement for thickness of the Au layer and the TTR measurement. In addition, the locations for the PMMA film measurement must be of uniform thickness since it is not possible to observe the PMMA film once the Au deposition process was complete. Figure 4.2 shows the extended thickness profile which was measured from one edge to the opposite edge on a sample (number: A3-004), which is depicted in Fig. 3.5.

The thickness measurement was obtained from points 1 to 9 with an interval length of 500 μm, and then with an interval length of 250 μm after point 9. As shown in Fig. 4.2, the film thickness was uniform as the sample approached the spinning axis of the spin-coater, while the thickness profile fluctuated when approaching the opposite edge. This was possibly due to the viscosity effect of the solution and the rectangle-shaped geometry of the silicon substrate. Thus, the uniform thickness area of PMMA film, as close to the spin-axis as possible, was chosen for TTR measurements. The length for the evaluation area was roughly 4 mm from the edge near the spin-axis, and consisted of seven points from 1 to 7 as shown in Fig. 3.5. After the thickness measurements were completed, the Au layers were sputter-coated onto the PMMA films simultaneously, and the result of the deposited Au layer is presented below.

Table 4.2 The thickness measurement uncertainty for PMMA films and Au layers

Sample number	PMMA Film			Au Layer		
	h_{PMMA} (nm)	$W_{h,95\%}$ (%)	N	h_{Au} (nm)	$W_{h,95\%}$ (%)	N
A1-005	39.7	0.22	9	470.4	1.01	6
A2-002	70.8	0.27	9	422.1	1.55	6
A3-004	121.7	0.62	9	416.3	0.65	6
A4-003	187.5	0.32	9	410.2	2.55	6
A5-004	305.2	0.44	9	414.6	5.13	6
A6-003	375.7	0.50	9	438.9	1.34	6
A7-006	596.6	0.28	9	396.9	1.42	6
A8-004	603.5	0.46	9	397.5	2.11	6
A9-004	720.1	2.24	9	405.7	2.45	6
A10-004	791.9	0.29	9	446.0	1.54	6
A11-002	1020.6	0.32	9	508.4	0.85	6
A11-023	1310.2	0.54	9	553.8	1.73	6
A11-102	2020.7	1.83	9	595.7	1.55	6
Thin Au-Si	–	–	–	420.8	1.64	6
Thick Au-Si	–	–	–	514.4	0.36	6

4.3 The Measured Thicknesses of Au Layers

A Dektak^{3}ST profilometer was used to measure the thickness of the sputter-coated Au layers on PMMA films, which was a necessary step due to the shadow mask technique. The thicknesses of the Au layers are plotted in Fig. 4.3. While the sputter coater was sputtering gold on the sample surfaces, an apparatus used to monitor thickness estimated the total thickness as 334 nm. However, it was found that the actual thickness of the Au layer was much deeper than the monitored value, as shown in Fig. 4.3 and Table 4.2.

For the uniformity of thickness in a sample, each sample has a different thickness due to the different locations of the samples in the sputter. Sample #A11-102 had thickest Au layer (upper dotted line: 596 nm) and sample #A7-006 had thinnest Au layer (lower dotted line: 397 nm). If the diameters of the gold targets were larger than the sample, then the Au layer would have had a more uniform thickness.

The scanning length using the profiler was determined to be one less than 1200 μm and the thickness of Au layer was evaluated within 100 μm length that contains the cross-sectional step to reduce the uncertainty that is attributed to waviness in the silicon substrate. Nevertheless, the maximum uncertainty of the measured thicknesses was 5.13% based on a confidence level of 95%, thus the measurement point for the TTR method was located at where the thickness of the Au layer was measured.

Each measurement using the profiler left a trace of the scanning tip on the surface of the Au layer, which was visible by using a 20× objective lens in the TTR system. The sets of measurement points in each sample were included in the thickness measurement area of PMMA film, and the TTR measurements were applied in a small area (1×3 mm), as close as possible to the center of the spin axis in order to minimize the uncertainties of the TTR measurements.

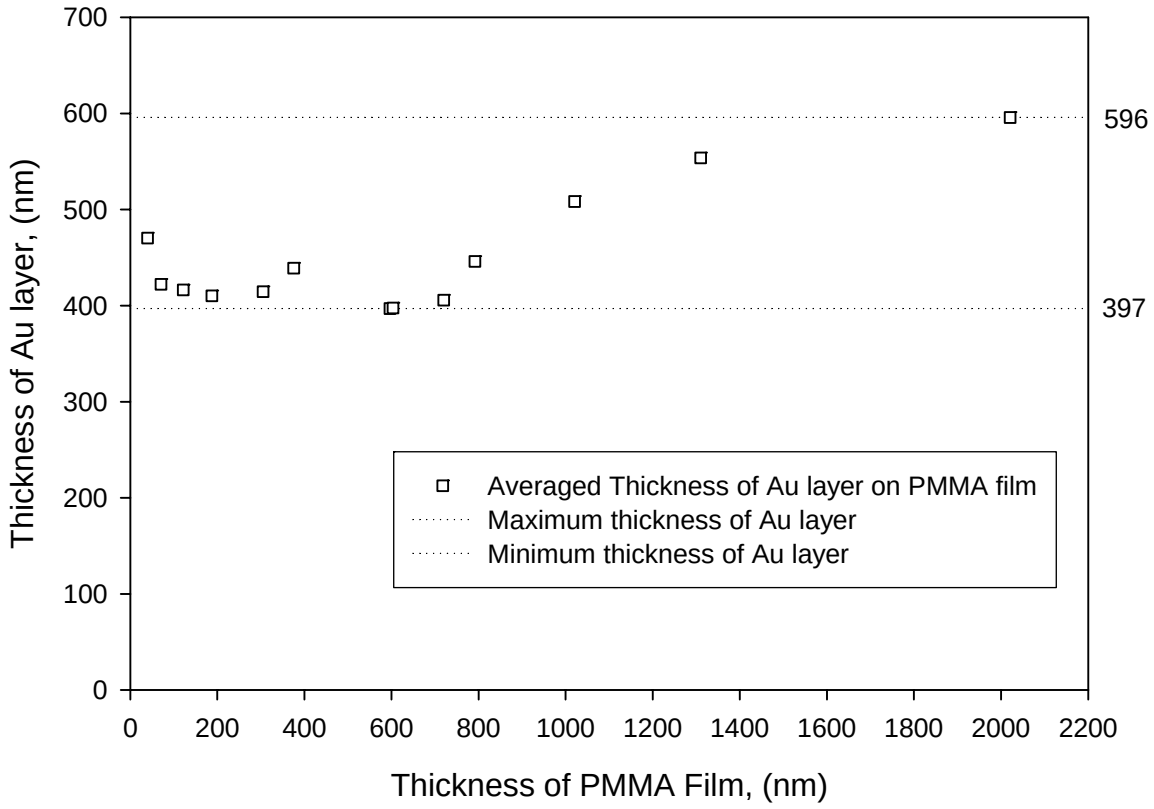

Fig. 4.3 Plot of thickness for Au layer on each PMMA film

4.4 TTR Measurement for Through-plane Thermal Conductivity of PMMA Film

The normalized TTR temperature responses obtained for the PMMA film samples are shown in Fig. 4.4. The maximum normalized temperatures in the samples were detected at 134 – 135 ns and the top Au layers started to cool after that time period. The nine samples, which have PMMA films with thickness ranging from 305.2 nm to 2.02 μm, showed indistinguishable slope during the cooling process. Meanwhile, an apparent change of the normalized temperature response was found in the samples that have PMMA films with thickness ranging from 39.7 nm to 187.5 nm. For instance, the ultra -thin (39.7 nm) PMMA film sample showed much faster temperature reduction than that of the other samples in the cooling process.

Figure 4.5 shows the matched numerical temperature response to each experimental response of the five representative samples obtained by varying the material thermal diffusivity in the numerical simulation until the numerical curve fits the experimental result within a 1% error. In Fig. 4.5, the black dotted line was the measured TTR responsivity that is normalized by the maximum temperature, and the red and blue colored lines are numerically computed responses.

Each TTR response curve consists of 1000 transient temperature responses as normalized temperature versus time. The 900 numerical response data in a curve were fitted to the TTR response curve that ranged from 0 ns to 344 ns. As shown in Figs. 4.4 and 4.5, the decay of the temperature response was faster for the sample with a thinner layer of PMMA film, which ranged from 187.5 nm to 39.7 nm. On the other hand,

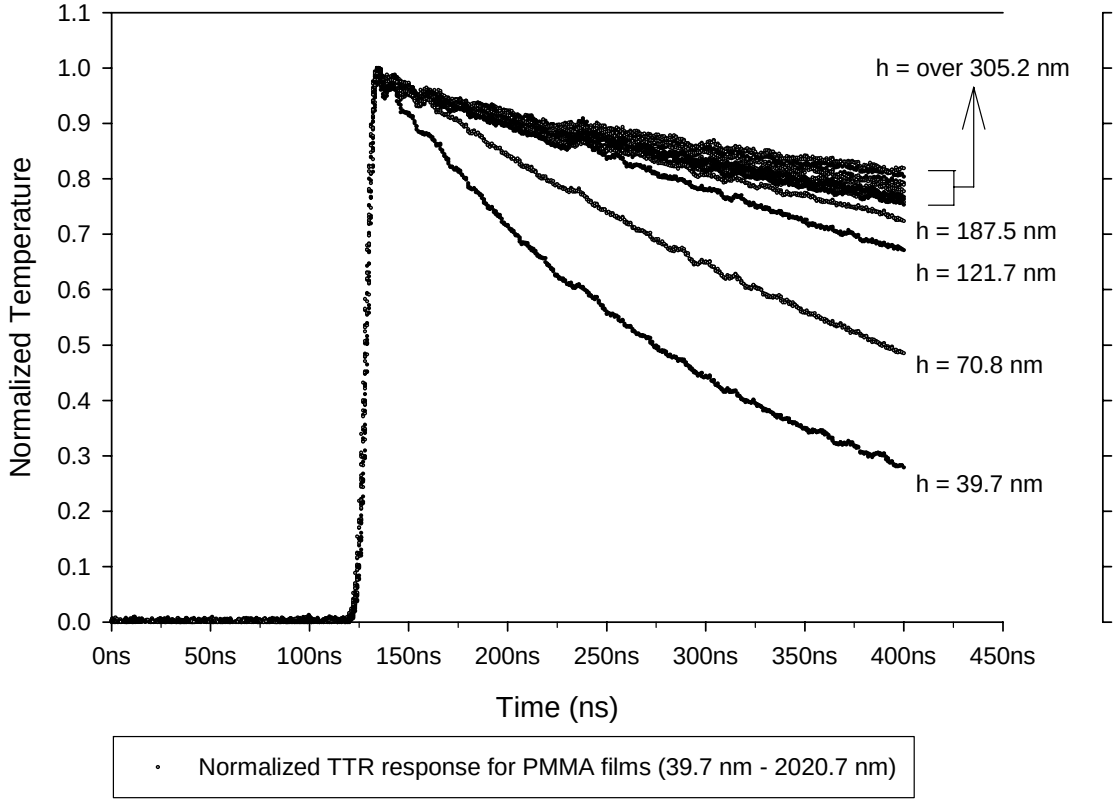

Fig. 4.4 Normalized TTR response for samples that have various thickness of PMMA films whose thickness ranged from 39.7 nm to 187.5 nm and from 305.2 nm to 2020.7 nm

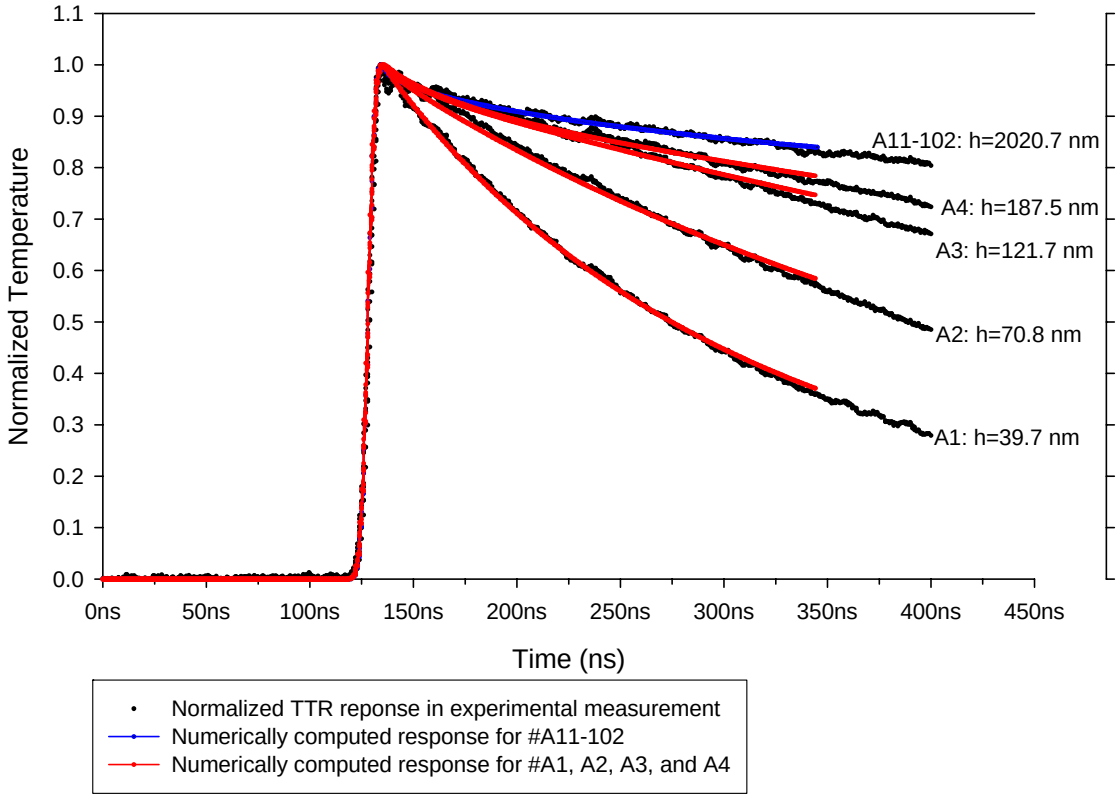

Fig. 4.5 Normalized TTR response and the matched numerical response within 1% error for four samples: A1-005, A2-002, A3-004, A4-003, and A11-102

the samples of PMMA film with thicknesses ranging from 2020.7 nm to 305.2 nm showed an almost constant decay of the temperature response.

The measured intrinsic thermal conductivities of PMMA films were plotted as shown in Fig. 4.6. As the film thickness decreased, a pronounced increase in the through-plane thermal conductivity was observed, and the thermal conductivity reached a maximum value of 0.72 W m^{-1} k^{-1} at a thickness of 39.7 nm. The average thermal conductivity in the three bulk thicknesses (1.02 μm, 1.31 μm, and 2.02 μm) was 0.21 W m^{-1} k^{-1}, which is a dotted line as reference. The intrinsic through-plane thermal conductivity of the embedded PMMA films started to increase at thicknesses less than 187.5 nm, and the measured values above that particular thickness remained constant at 0.21 W m^{-1} k^{-1}. Detailed values are presented in Table 4.3.

With the TTR method, the two unknown properties, the intrinsic through-plane thermal conductivity and interface thermal resistance R_{I1}, were measured in each of the thirteen samples. Most of the measured R_{I1} values at each location ranged between 4.7×10^{-8} m^2KW^{-1} and 7.9×10^{-8} m^2 K W^{-1} without thickness dependence. The measured interface thermal resistance (R_{I1}) was relatively high when compared with R_{I2} (0.5×10^{-8} m^2 K W^{-1}), which was the interface resistance between the PMMA film and silicon substrate, and varied on measurement location. Samples A6-003 and A10-004 showed the averaged interface thermal resistance R_{I1} value as 1.62×10^{-8} m^2 K W^{-1} and 1.50×10^{-8} m^2 K W^{-1}, respectively, while an averaged R_{I1} value for sample A5-004 was 7.88×10^{-8} m^2 K W^{-1}. It is suspected that the reason can be attributed to weak adhesion between the Au layer and PMMA film.

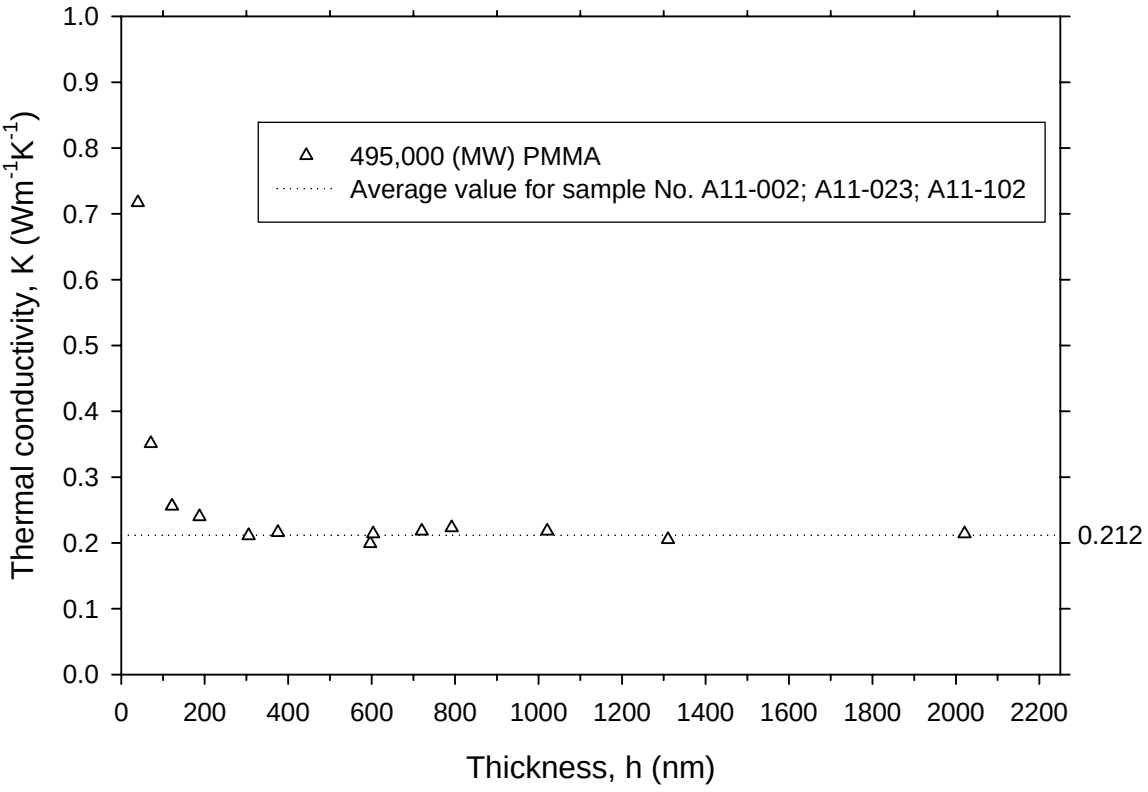

Fig. 4.6 Intrinsic thermal conductivity versus film thickness of PMMA film measured by TTR method

Table 4.3 Intrinsic through-plane thermal conductivity versus thickness of PMMA film and interface thermal resistance (R_{I1}) using the TTR measurement

Sample number	K_{PMMA} ($Wm^{-1}K^{-1}$)	R_{I1} (10^{-8} m^2KW^{-1})	W_K (%)	h_{PMMA} (nm)	h_{Au} (nm)
A1-005	0.717	4.72	3.94	39.7	470.4
A2-002	0.351	4.71	4.11	70.8	422.1
A3-004	0.256	6.36	3.85	121.7	416.3
A4-003	0.240	6.04	5.96	187.5	410.2
A5-004	0.211	7.88	9.11	305.2	414.6
A6-003	0.216	1.62	10.91	375.7	438.9
A7-006	0.199	6.33	8.53	596.6	396.9
A8-004	0.214	7.17	8.06	603.5	397.5
A9-004	0.218	7.41	7.78	720.1	405.7
A10-004	0.223	1.50	10.11	791.9	446.0
A11-002	0.218	4.74	9.77	1020.6	508.4
A11-023	0.205	3.94	10.56	1310.2	553.8
A11-102	0.214	4.71	11.92	2020.7	595.7

In order to confirm the first thickness at which the increased thermal conductivity was observed, the TTR measurement was performed at seven different locations in sample number A4-003, with a total of 50,000 shots for the heating and probing laser. The measured value showed a 13.3% increase in the 187.5 nm PMMA film compared with an average value of K (0.212 W $m^{-1} K^{-1}$) measured in thick PMMA films. Decreasing the film thickness from 187.5 nm caused an increase for the thermal conductivity that was definitely observable.

The intrinsic through-plane thermal conductivity was 0.256 W $m^{-1} K^{-1}$ at 121.7 nm, 0.351 W $m^{-1} K^{-1}$ at 70.8 nm, and 0.717 W $m^{-1} K^{-1}$ at 39.7 nm PMMA film as shown in Table 4.3. The normalized thermal conductivity, normalized by the averaged value of K_{bulk} (0.212 W $m^{-1} K^{-1}$) is shown in Fig. 4.7. When these values were normalized by the measured K_{bulk} (0.212 W $m^{-1} K^{-1}$), it is worth mentioning that the trend of the measured through-plane thermal conductivity was very similar to the one for the acoustic speed measured by Lee et al.[17].

The results showed that a 238.4% and a 65.7% increase in the through-plane thermal conductivity were found for the 39.7 nm and 70.8 nm PMMA film, respectively, and a 20.5% and a 13.3% increase was found for each 121.7 nm and 187.5 nm film, respectively. On the other hand, the through-plane acoustic speed increased approximately 187% at 22 nm, 118% at 30 nm, 75% at 36 nm, and 9% at 40 nm for the PMMA films on an aluminum layer[17].

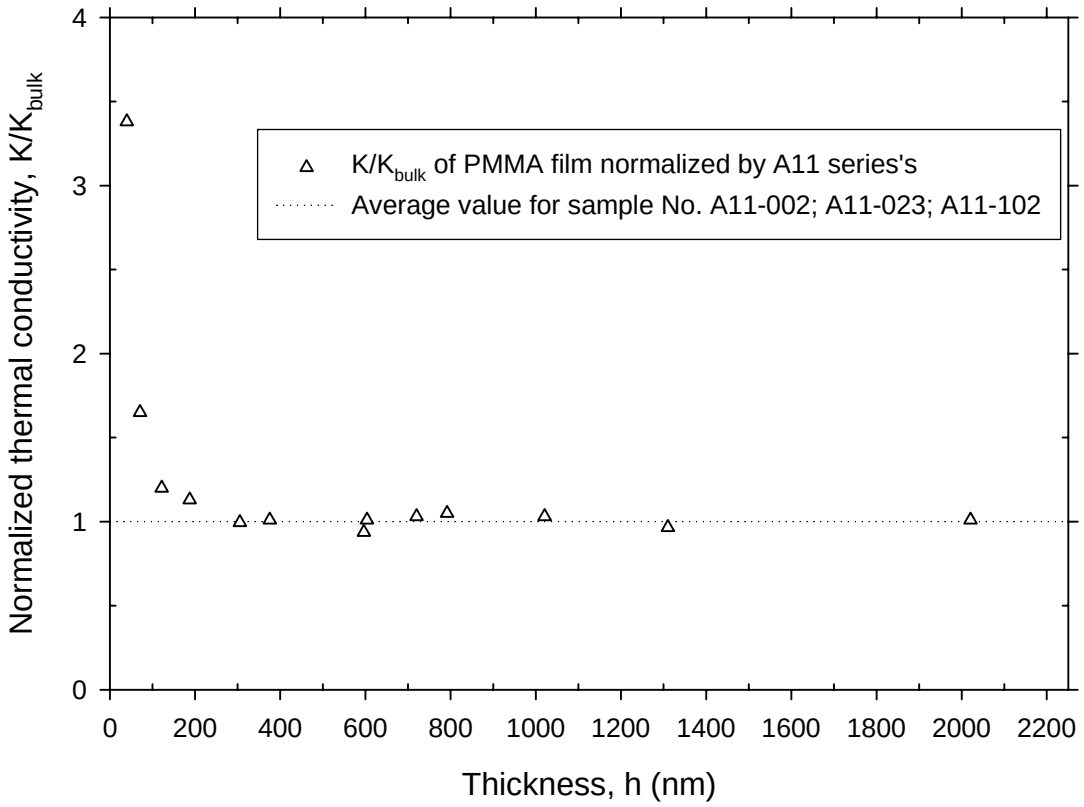

Fig. 4.7 Normalized thermal conductivity by average values K (0.212 $Wm^{-1}K^{-1}$) of bulk PMMA film samples

If the measured thermal conductivity was decreased by decreasing the film thickness, one may conclude that the reason might be due to scattering of the thermal carriers since the mobility of phonons determines the thermal transport properties in polymer material, and the mobility of the phonon might be affected by scattering due to defects and internal or external boundaries. However, the increased thermal conductivity of PMMA film with decreasing film thickness indicated that phonon scattering effects are diminished for thin PMMA film in this study.

In addition, the mean free path (l) for acoustic phonons in bulk PMMA material can be calculated from the thermal conductivity (K), ρC_p, and acoustic speed (v) based on kinetic theory. The calculated mean free path (l) was approximately 1.2 Å in bulk PMMA material, and the value was calculated to 1.3 Å in thick (1 μm – 2 μm) PMMA films. In addition, the available maximum mean free path in ultra-thin (h = 40 nm) PMMA film was 4.1 Å based on the measured thermal conductivity and the acoustic speed reported by Lee et al.[17].

Even if the available maximum mean free path (l = 4.1 Å) for acoustic phonons is considered for the microscale regime criteria that Flik et al.[12] presented, the ratio l/h ($\approx$ 0.01) is too small to anticipate boundary scattering of phonons in the thinnest film (h = 40 nm). The authors showed that if $h < 7l$, the microscale regime (size dependent transport properties) has to be used in both metallic and dielectric materials. Thus, author safely conclude that the “size effect” caused by phonon scattering due to boundary scattering was not found in the thickness range from thick (2 μm) to ultra-thin

thicknesses (40 nm), but that internal scattering (atom-to-atom) might be the dominate mode.

However, if the microstructure of PMMA film changes near the substrate regime or the mobility of molecules changes due to an interaction between the PMMA film and substrate, the thermal conductivity for the thin film would have thickness dependence as it approaches the interface. Thus, it is highlighted that the starting points at which the increases, in measured thermal conductivity in this study and acoustic speed study by Lee et al.[17], occurred at difference film thicknesses due to the influence caused by the film/substrate interface.

The reason for the increase in both thermal conductivity and acoustic speed for ultra-thin and thin PMMA films can be attributed to the substrate effect caused by attractive interaction between the PMMA film and the native oxide on the (100) silicon wafer. As presented in the literature, Lee et al. [17] reported a difference of acoustic speeds between an aluminum substrate and an oxide layer on an aluminum substrate. They found a 10%-20% increase in the acoustic speed for films thinner than 60 nm on the aluminum oxide layer, and thought that it was ascribed to the uncertainty of the thickness measurement for PMMA films. However, researchers have shown experimental data for T_g for PMMA films that indicated thickness dependence and the influenced caused by the substrate.

Keddie et al. [14] observed that the T_g for PMMA film less than 100 nm in thickness had a different trend on a Au layer than on a native oxide layer. Since the T_g of polymers is related to the mobility of the polymer film, the fact that the T_g of thin

PMMA film increases below 100 nm deposited on a native oxide silicon wafer while the T_g for the PMMA on a gold surface decreases with decreasing film thickness seems to correlate with the result of this study. Fryer et al.[15] showed that the deviation of the T_g values for thin films compared to the bulk values increased with decreasing film thickness at high interfacial energy between polymer film and substrate. Diakoumakos, C. D. and Raptis, I.[16] also observed that *Tg* for PMMA films increased by decreasing film thickness under 200 nm, and reported that the T_g of ultra-thin (sub 100 nm) PMMA film was significantly increased and deviated substantially, by approximately 30˚C, from the value for thickn PMMA film. These studies with respect to the behavior of T_g for PMMA films on various substrates and film thicknesses show the interaction between the PMMA film and substrate, which is related to the behavior of the modulus.

As mentioned, one may conclude that the substrate effect for spin-coated polymer films exists within some thickness regime. In this study, since the substrates contained an native oxide on to the (100) silicon wafers, which was different from the film substrate (Al or Al_2O_3) employed by Lee et al.[17], it was assumed that the acoustic speed profile of the currently studied samples would also be different from that of Lee et al.[17]. Unfortunately, no experimental data exist in measurements of both the acoustic speed and the thermal conductivity for thin PMMA films with similar substrates to this study.

However, a more detailed surface effect regime for PMMA film was reported by Priestley et al.[29,30]. They measured the rate of structure relaxation for PMMA films at a free surface and at a silica substrate interface and showed that the reduction of the

structural relaxation rates at 305 K slowly begins at a distance between 100 nm and 250 nm from the substrate interface as shown in Fig. 4.8. Thickness regions less than 25 nm from the substrate interface exhibited a factor of 15 reduction in relaxation rate relative to bulk values. This reduction of the structure relaxation rate was evidence of confinement on physical aging due to attractive PMMA film-silica substrate interaction, which was hydrogen bond formation.

The reduction of the physical aging rate means confinement of segmental mobility and an increased modulus, which was attributed to the hydrogen bonds[29,31]. Since the glassy-state structural relaxation is more sensitive than T_g towards surface interfacial effects, their results are evidence for the substrate effect on subsegmental structure of PMMA film near the silica substrate interface.

In this study, the first observation of thermal conductivity increase was found in sample number A4-003, a thickness of 187.5 nm and 13.3% increase observed at this thickness. A distinct increase in intrinsic through-plane thermal conductivity for the PMMA film was observed in thicknesses less than 71 nm. The measured thermal conductivity for this study shows good agreement with the results presented by Priestley et al.[29,30], suggesting a reasonable explanation for the trend for T_g values and the increase in both acoustic speed profile and mass density by decreasing thickness near the silica substrate.

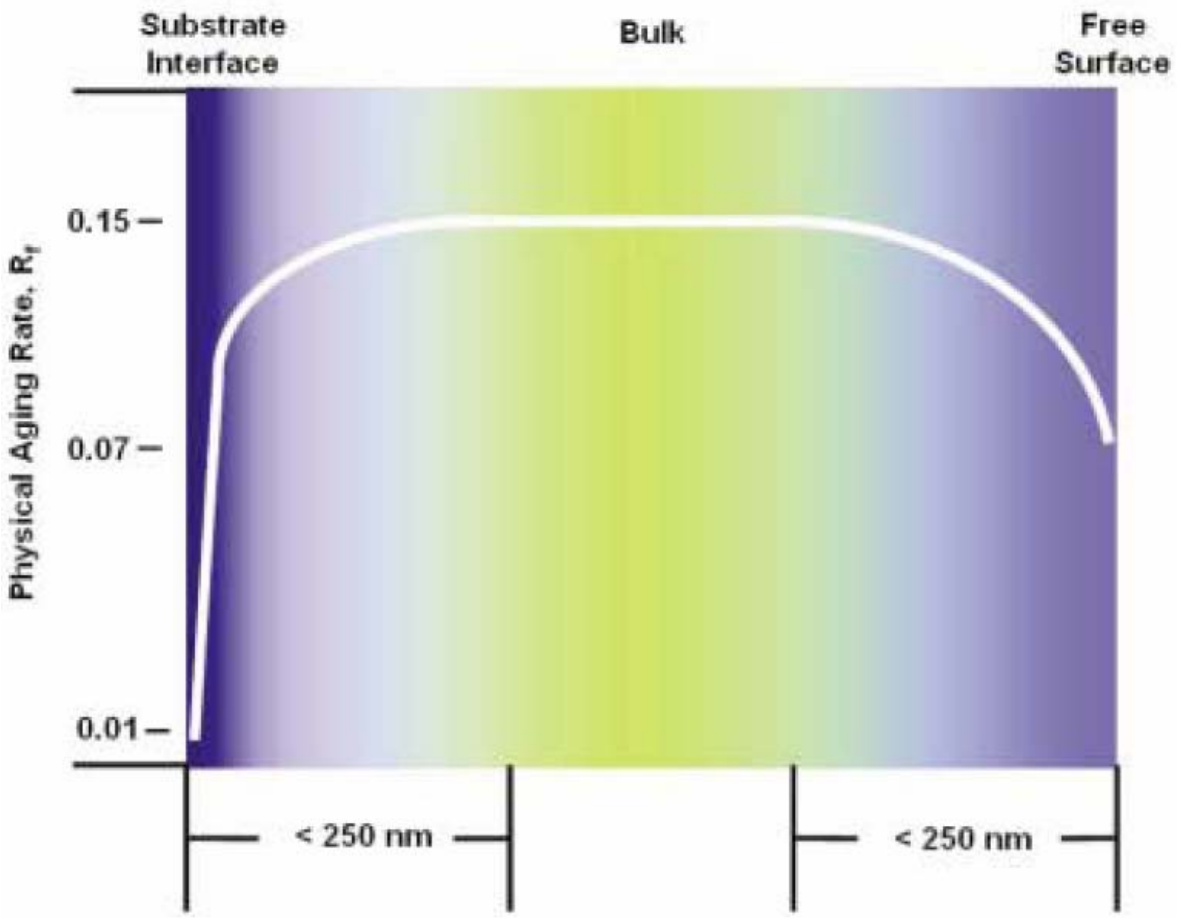

Fig. 4.8 Measured physical aging rate of PMMA on silica substrate at 305 K depending on film thickness by Priestley et al.[29]

4.5 Measurement Uncertainty

The estimation of uncertainty values was based on the analysis developed by Kline and McClintock[32] with a confidence level of 95% (or 20:1 odds). The method was based on the uncertainties in the primary measurements, such as the thickness measurements of the PMMA film and the Au layer, and then, the uncertainty for the thickness of each layer was considered for the uncertainty of thermal conductivity in the TTR measurement.

In the TTR measurements, M.G. Burzo [33] presented an uncertainty analysis for numerical procedures and experimental work because the uncertainties caused by the numerical procedures are attributed to the uncertainties in the process of matching the experimental temperature transient response with the numerical solution of the heat equation. In this study, uncertainty analysis for the thermal conductivity measurement followed M. G. Burzo's[25,33] description of uncertainty analysis in the TTR measurement.

Total uncertainty, W_k, for thermal conductivity measurement was presented by Burzo as follows:

$$W_k = W_{total} = \frac{W_\theta}{\Omega_K} \tag{4.1}$$

where W_θ is the uncertainty in the transient normalized surface temperature response (θ) and Ω_K is responsivity for thermal conductivity K from the responsivity of the transient temperature response as follows:

$$W_\theta = \sqrt{(W_{num})^2 + (W_{\exp})^2} \tag{4.2}$$

$$\Omega_V = V \frac{\partial \theta}{\partial V} \tag{4.3}$$

where V is one of the following variables: thermal conductivity K, thickness of the layer h, imaginary part of the refractive index of the top layer k, real part of the refractive index of the top layer n, or the thermal capacitance ρC_p.

Thus, Ω_K is calculated numerically from Eq. (4.3), and the other responsivities of the temperature response for the variables are shown in Table 4.4. Thus, the numerically based uncertainties W_{num} and experimentally based uncertainty W_{exp} are estimated for W_θ.

Table 4.4 Responsivity of the TTR setup parameters for materials in samples

Sample number	Ω_k	Ω_K		$\Omega_{\rho Cp}$			Ω_h	
	Au	Au	Si	Au	PMMA	Si	Au	PMMA
A1-005	0.013	0.101	0.052	0.320	0.006	0.052	0.311	0.000
A2-002	0.012	0.091	0.028	0.334	0.017	0.026	0.369	0.000
A3-004	0.012	0.088	0.009	0.311	0.041	0.009	0.458	0.000
A4-003	0.012	0.085	0.003	0.258	0.064	0.003	0.377	0.166
A5-004	0.012	0.087	0.000	0.207	0.091	0.000	0.147	0.050
A6-003	0.013	0.096	0.000	0.196	0.099	0.000	0.139	0.000
A7-006	0.012	0.084	0.000	0.208	0.108	0.000	0.159	0.000
A8-004	0.012	0.086	0.000	0.211	0.110	0.000	0.161	0.000
A9-004	0.012	0.083	0.000	0.205	0.111	0.000	0.000	0.000
A10-004	0.013	0.099	0.000	0.193	0.106	0.000	0.210	0.000
A11-002	0.013	0.113	0.000	0.161	0.100	0.000	0.231	0.000
A11-023	0.013	0.113	0.000	0.124	0.094	0.000	0.231	0.000
A11-102	0.014	0.123	0.000	0.114	0.090	0.000	0.251	0.000

The uncertainty of the matching procedure W_{num} was estimated by calculating the standard deviation between the experimental and numerical transient temperature responses in the effective time range in each TTR measurement. The result of W_{num} is shown in Table 4.5. The experimental uncertainty W_{exp} is calculated as follows:

$$W_{\exp} = \sqrt{(W_{TTR})^2 + (\Omega_h W_h)^2 + (\Omega_K W_K)^2 + \left(\Omega_{\rho C_p} W_{\rho C_p}\right)^2 + (\Omega_n W_n)^2 + (\Omega_k W_k)^2} \quad (4.4)$$

Each sample was tested using the TTR method in at least three different locations within 1×3 mm on the sample. At each location, the heating laser was pulsed 500 times for the samples that ranged from A3 to A11 and 750 times for the samples A1 and A2. Then, the obtained transient responses were averaged for the number times the laser was pulsed, either 500 times or 750 times.

The standard deviation of the obtained transient responses versus time was calculated for the different locations in a sample. Thus, the uncertainty W_{TTR} was estimated from the time-averaged standard deviation. The result of W_{TTR} is shown in Table 4.5.

Table 4.5 The TTR measurement uncertainties

Sample No.	h_{PMMA} (nm)	K_{PMMA} ($Wm^{-1}K^{-1}$)	Ω_K –	W_{TTR} (%)	W_{num} (%)	W_{exp} (%)	W_{θ} (%)	W_{TOTAL} (%)
A1-005	39.7	0.717	0.262	0.442	0.74	0.91	1.17	4.47
A2-002	70.8	0.351	0.307	0.314	0.99	0.99	1.40	4.56
A3-004	121.7	0.256	0.299	0.382	0.95	0.93	1.33	4.44
A4-003	187.5	0.240	0.229	0.335	0.81	1.33	1.56	6.82
A5-004	305.2	0.211	0.135	0.536	0.69	1.14	1.33	9.87
A6-003	375.7	0.216	0.115	0.394	1.08	0.82	1.36	11.81
A7-006	596.6	0.199	0.109	0.426	0.65	0.87	1.09	9.97
A8-004	603.5	0.214	0.110	0.272	0.61	0.86	1.05	9.59
A9-004	720.1	0.218	0.111	0.411	0.60	0.84	1.03	9.31
A10-004	791.9	0.223	0.107	0.565	0.72	0.97	1.21	11.30
A11-002	1020.6	0.218	0.100	0.409	0.72	0.82	1.09	10.92
A11-023	1310.2	0.205	0.094	0.296	0.73	0.80	1.08	11.52
A11-102	2020.7	0.214	0.090	0.455	0.76	0.87	1.15	12.76

The thickness measurement was performed by using an ellipsometer and profiler that have at least a 1Å resolution and a better than 10Å repeatability. The uncertainty W_h of both the Au layer and PMMA film was calculated based on the accuracy of the thickness measurements, which is between 20 and 40Å for the profiler and less than 10Å for the ellipsometer. The calculated W_h are shown in Table 4.2. The uncertainty in the thermal conductivity W_K for the Au layer and silicon wafer is considered to be 3% each.

The mass density and heat capacity of PMMA film does not change significantly with the film thickness. However, the mass density of ultra-thin PMMA film has thickness dependence as shown in the literature review. Thus, the uncertainty $W_{\rho Cp}$ of PMMA films was estimated to be 10% in the samples that have thickness less than 250 nm, and 5% in the samples that have thickness ranged from 305 nm to 2.02 μm.

The ρC_p of the Au layer has a slight effect depending on the sputtering procedure. This value was measured by the TTR method using an Au layer-silicon substrate sample, and the uncertainty $W_{\rho Cp}$ of the Au layer was estimated to be 2% in this study.

The uncertainty of W_k is insignificant for the sample and can be neglected, as can the sensitivity of the TTR response to k_{Au} because the responsivity Ω_k for the Au layer is very low (around 0.01), and it was measured using the ellipsometer and contained a less than 5% measurement error. The responsivity Ω_n for the real part of the refractive index is zero because the TTR method measures relative changes of reflectivity with temperature. Thus, the uncertainty W_n for the Au layer is negligible.

The responsivity of each material is numerically calculated and is shown in Table 4.4. The total uncertainty for the measured thermal conductivity is shown in Table 4.5. The ultra-thin (sub-100 nm) PMMA film samples have 4.47% and 4.56% uncertainties for the sample number A1-005 and A2-002 respectively, while bulk thick (over 1 μm) PMMA films have 10.92%, 11.52%, and 12.76% uncertainties for the sample number A11-002, A11-023, and A11-102 in the measured thermal conductivity respectively.

4.6 Summary of the Result

For experimental investigation of size effects on thermal conductivity for ultra-thin amorphous poly(methylmethacrylate) (PMMA) films, PMMA films (with a molecular weight of 495000 obtained from MicroChem) were spin-coated onto (100) silicon wafers using an anisole solvent. Film thickness was varied by changing the concentration of the solution, and PMMA films with thicknesses ranging from 40 nm to 2.02 μm were successfully fabricated as samples in this study. In order to apply the TTR method, a gold (Au) layer was deposited onto PMMA films for the absorption layer of the heating laser using a Sputter Coater and the measured thicknesses of the Au layers were between 396.9 nm and 595.7 nm.

The result of this experimental measurement for thermal conductivity on ultra-thin and thin PMMA films demonstrated that the intrinsic through-plane thermal conductivity of thin PMMA films increased with decreasing film thickness below 187.5 nm. The thermal conductivity of ultra-thin PMMA films showed a precipitous increase within sub 100 nm thickness.

CHAPTER V

CONCLUSION AND RECOMMENDATIONS

The intrinsic through-plane thermal conductivity for PMMA films with thicknesses ranging from ultra-thin (40 nm) to bulk film (2 μm) was experimentally measured with the TTR method. The results showed a distinct increase in the thermal conductivity for PMMA films as the thickness decreased and the first deviation from the bulk value was observed for films approaching a thickness of 188 nm.

Until now, researchers have shown a size effect on thermal conductivity that decreased as the film thickness was reduced in metallic or dielectric materials; however, the behavior of thermal conductivity in amorphous PMMA film does not correlate with the size effect. In this study, a reduction in thermal conductivity values due to phonon scattering from boundary scattering was not found in the thickness range tested.

The intrinsic thermal conductivity for thin PMMA film on native oxide of (100) silicon wafer increased by 238% and 66% at 40 nm and 71 nm thicknesses, respectively. This is in comparison to measured values for bulk PMMA films. The increase for thermal conductivity was attributed to the attractive interaction between the PMMA film and the native oxide present on the silicon wafer, which contained hydrogen bonds that confined the segmental mobility of the polymer.

Thus, author suspect that this caused an increase in the mass density and acoustic speed, which then caused an increase in the thermal conductivity. These

observations should cause a careful consideration of the substrate effect for thin polymer films for both thermophysical and mechanical properties.

REFERENCES

[1] G. Binnig, M. Despont, U. Drechsler, W. Haberle, M. Lutwyche, P. Vettiger, H.J. Mamin, B.W. Chui and T.W. Kenny, Ultrahigh-density atomic force microscopy data storage with erase capability, Applied Physics Letters 74 (9) (1999) 1329-1331.

[2] P. Vettiger, M. Despont, U. Drechsler, U. Durig, W. Haberle, M.I. Lutwyche, H.E. Rothuizen, R. Stutz, R. Widmer and G.K. Binnig, The "Millipede" - More than one thousand tips for future AFM data storage, IBM Journal of Research and Development 44 (3) (2000) 323-340.

[3] U. Durig, G. Cross, M. Despont, U. Drechsler, W. Haberle, M.I. Lutwyche, H. Rothuizen, R. Stutz, R. Widmer, P. Vettiger, G.K. Binnig, W.P. King and K.E. Goodson, "Millipede" - an AFM data storage system at the frontier of nanotribology, Tribology Letters 9 (1-2) (2000) 25-32.

[4] M.G. Burzo, P.L. Komarov and P.E. Raad, Minimizing the uncertainties associated with the measurement of thermal properties by the transient thermo-reflectance method, IEEE Transactions on Components and Packaging Technologies 28 (1) (2005) 39-44.

[5] W.P. King, T.W. Kenny, K.E. Goodson, G.L.W. Cross, M. Despont, U.T. Durig, H. Rothuizen, G. Binnig and P. Vettiger, Design of atomic force microscope cantilevers for combined thermomechanical writing and thermal reading in array operation, Journal of Microelectromechanical Systems 11 (6) (2002) 765-774.

[6] E. Grochowski and R.F. Hoyt, Future trends in hard disk drives, IEEE Transactions on Magnetics 32 (3) (1996) 1850-1854.

[7] R.P. Ried, J. Mamin, B.D. Terris, L.S. Fan and D. Rugar, 6-MHz 2-N/m piezoresistive atomic-force-microscope cantilevers with INCISIVE tips, Journal of Microelectromechanical Systems 6 (4) (1997) 294-302.

[8] W.P. King and K.E. Goodson, Thermal writing and nanoimaging with a heated atomic force microscope cantilever, Journal of Heat Transfer-Transactions of the Asme 124 (4) (2002) 597-597.

[9] W.M. Rohsenow and H.Y. Choi, Heat, Mass, and Momentum Transfer, Prentice-Hall, Englewood Cliffs, NJ, 1961.

[10] D.G. Cahill, H.E. Fischer, T. Klitsner, E.T. Swartz and R.O. Pohl, Thermal-conductivity of thin-films - measurements and understanding, Journal of Vacuum Science & Technology a-Vacuum Surfaces and Films 7 (3) (1989) 1259-1266.

[11] M.A. Omar, Elementary Solid State Physics, Addison-Wesley Publishing Company, Massachusetts, 1993.

[12] M.I. Flik, B.I. Choi and K.E. Goodson, Heat-transfer regimes in microstructures, Journal of Heat Transfer-Transactions of the Asme 114 (3) (1992) 666-674.

[13] A. van der Lee, L. Hamon, Y. Holl and Y. Grohens, Density profiles in thin PMMA supported films investigated by X-ray reflectometry, Langmuir 17 (24) (2001) 7664-7669.

[14] J.L. Keddie, R.A.L. Jones and R.A. Cory, Interface and surface effects on the glass-transition temperature in thin polymer-films, Faraday Discussions (98) (1994) 219-230.

[15] D.S. Fryer, R.D. Peters, E.J. Kim, J.E. Tomaszewski, J.J. de Pablo, P.F. Nealey, C.C. White and W.L. Wu, Dependence of the glass transition temperature of polymer films on interfacial energy and thickness, Macromolecules 34 (16) (2001) 5627-5634.

[16] C.D. Diakoumakos and I. Raptis, In situ monitoring of thermal transitions in thin polymeric films via optical interferometry, Polymer 44 (1) (2003) 251-260.

[17] Y.C. Lee, K.C. Bretz, F.W. Wise and W. Sachse, Picosecond acoustic measurements of longitudinal wave velocity of submicron polymer films, Applied Physics Letters 69 (12) (1996) 1692-1694.

[18] C.M. Stafford, B.D. Vogt, C. Harrison, D. Julthongpiput and R. Huang, Elastic moduli of ultrathin amorphous polymer films, Macromolecules 39 (15) (2006) 5095-5099.

[19] C.M. Stafford, C. Harrison, K.L. Beers, A. Karim, E.J. Amis, M.R. Vanlandingham, H.C. Kim, W. Volksen, R.D. Miller and E.E. Simonyi, A buckling-based metrology for measuring the elastic moduli of polymeric thin films, Nature Materials 3 (8) (2004) 545-550.

[20] R. Frank, V. Drach and J. Fricke, Determination of thermal-conductivity and specific-heat by a combined 3-Omega decay technique, Review of Scientific Instruments 64 (3) (1993) 760-765.

[21] D.C. Chu, M. Touzelbaev, K.E. Goodson, S. Babin and R.F. Pease, Thermal conductivity measurements of thin-film resist, Journal of Vacuum Science & Technology B 19 (6) (2001) 2874-2877.

[22] M.G. Burzo, P.L. Komarov and P.E. Raad, A study of the effect of surface metalization on thermal conductivity measurements by the transient thermo-reflectance method, Journal of Heat Transfer-Transactions of the Asme 124 (6) (2002) 1009-1018.

[23] Y.N. Srivastava, A.P. Gadre, T. Hylton, A.H. Monica, T.W. Schneider, R.C. White, M. Paranjape and J.F. Currie, Polymethylmethacry ate membrane for fluid encapsulation and release in microfluidic systems, Journal of Vacuum Science & Technology A 22 (3) (2004) 1067-1072.

[24] M.G. Burzo, P.L. Komarov and P.E. Raad, Influence of the metallic absorption layer on the quality of thermal conductivity measurements by the transient thermo-reflectance method, Microelectronics Journal 33 (9) (2002) 697-703.

[25] P.L. Komarov, M.G. Burzo, G. Kaytaz and P.E. Raad, Transient thermo-reflectance measurements of the thermal conductivity and interface resistance of metallized natural and isotopically-pure silicon, Microelectronics Journal 34 (12) (2003) 1115-1118.

[26] T.Q. Qiu and C.L. Tien, Short-pulse laser-heating on metals, International Journal of Heat and Mass Transfer 35 (3) (1992) 719-726.

[27] T.Q. Qiu and C.L. Tien, Femtosecond laser-heating of multilayer metals .1. Analysis, International Journal of Heat and Mass Transfer 37 (17) (1994) 2789-2797.

[28] P.L. Komarov and P.E. Raad, Performance analysis of the transient thermo-reflectance method for measuring the thermal conductivity of single layer materials, International Journal of Heat and Mass Transfer 47 (14-16) (2004) 3233-3244.

[29] R.D. Priestley, C.J. Ellison, L.J. Broadbelt and J.M. Torkelson, Structural relaxation of polymer glasses at surfaces, interfaces and in between, Science 309 (5733) (2005) 456-459.

[30] R.D. Priestley, L.J. Broadbelt and J.M. Torkelson, Physical aging of ultrathin polymer films above and below the bulk glass transition temperature: Effects of attractive vs neutral polymer-substrate interactions measured by fluorescence, Macromolecules 38 (3) (2005) 654-657.

[31] Y. Huang and D.R. Paul, Experimental methods for tracking physical aging of thin glassy polymer films by gas permeation, Journal of Membrane Science 244 (1-2) (2004) 167-178.

[32] S.J. Kline and F.A. McClintock, Describing uncertainties in single-sample experiments, Mechanical Engineering 75 (1) (1953) 3-8.

[33] M.G. Burzo, Transient thermoreflectance measurements of the thermal properties of metallized thin-film electronics materials, Ph.D. Dissertation, Mechanical Engineering, Southern Methodist University, 2001.

VITA

Name: Ick Chan Kim

Address: 1800 Holleman Drive #1312
College Station, TX 77840

Email Address: ickchan@gmail.com

Education: B.En., Mechanical Engineering, In-Ha University, Korea, 1999
M.S., Mechanical Engineering, Texas A&M University, 2007